NTNU

Norwegian University of
Science and Technology

Optimization of volumetric modulated arc therapy of cervical cancer

Retrospective treatment planning for simultaneous integrated boost, with and without flattening filter

Even Thorstensen Andersen

Master of Science in Physics and Mathematics
Submission date: June 2018
Supervisor: Anne Beate Langeland Marthinsen, IFY
Co-supervisor: Josefine Ståhl Kornerup, St. Olavs Hospital

Norwegian University of Science and Technology
Department of Physics

Abstract

The traditional treatment of cervical cancer is external beam radiotherapy (EBRT) combined with brachytherapy (BT) and concomitant chemotherapy. BT is used to boost the primary tumor in the pelvic area towards the end of the EBRT. In patients where the cancer has metastasized to nearby lymph nodes, external radiation boost is given to the affected lymph nodes. Traditionally this lymph node boost has been given sequentially, that is, after the EBRT of the primary pelvic target. Modern treatment techniques, such as intensity modulated radiotherapy (IMRT) and volumetric modulated arc therapy (VMAT), have made it easier to deliver the boost at the same time as the EBRT of the pelvic target. This is called simultaneous integrated boost (SIB). VMAT treatment with SIB is now a common practice for EBRT of cervical cancer patients with regional affected lymph nodes.

The most commonly used modality for EBRT is photon radiation (6MV), which is generated in a linear accelerator (linac) where several mechanical elements are used to generate and shape the photon beam properly. One of these is the flattening filter, which is used to flatten the fluence profile of the beam. This filter may also be removed, which will preserve the cone shaped profile of the photon beam in a so-called flattening filter-free (FFF) beam. EBRT with FFF beams is given with higher dose rate (and possibly reduced treatment time) than beams with flattening filter, and can be used for treatment of several cancer types.

In this master project 15 patients which had previously received radiotherapy for cervical cancer at St. Olavs Hospital, with EBRT, BT and sequential EBRT boosting of metastatic lymph nodes, were included. In this study, both standard 6MV VMAT and FFF VMAT treatment plans including SIB were retrospectively made for all patients. The standard 6MV plans and the FFF plans were evaluated and compared in terms of whether or not they could fulfill defined dose constraints, in addition to comparison of the homogeneity and conformity of the plans. All plans were further delivered to a quality assurance (QA) phantom, to assess how well these plans could be delivered by

a clinical linac. Several parameters were extracted from the QA measurements, and the 6MV and FFF plans were further compared with respect to these. The aim was to examine whether or not FFF plans could be delivered with the same accuracy from a linac, as the corresponding 6MV plans.

Both standard 6MV and FFF treatment plans were satisfactory with respect to dose coverage of target volumes, and they were about equal in sparing of nearby organs at risk, when evaluating them in a treatment planning system. However, data from the QA measurements showed that the 6MV plans were more accurately delivered to the QA phantom, compared to the corresponding FFF treatment plans. Therefore, for the complex and inhomogeneous volumes to be irradiated in patients with cervical cancer with lymph node metastases, the standard 6MV VMAT SIB plans are preferred to FFF plans.

Sammendrag

Den tradisjonelle behandlingen av livmorhalskreft er ekstern stråleterapi (EBRT) kombinert med brachyterapi (BT) og konkomitant kjemoterapi. BT brukes som en boost til primærtumoren i bekkenregionen mot slutten av EBRT. For pasienter der kreften har metastasert til nærliggende lymfeknuter, blir en ekstern boost gitt til affekterte lymfeknuter. Tradisjonelt har denne boosten til lymfeknutene vært gitt sekvensielt, det vil si etter EBRT av det primære målvolumet i bekkenet. Moderne behandlingsteknikker som IMRT og VMAT har gjort det enklere å levere denne eksterne boosten samtidig med EBRT av målvolumet i bekkenet. Dette kalles simultanintegrert boost (SIB). VMAT behandling med SIB er nå en vanlig praksis for EBRT av pasienter med livmorhalskreft med regionalt affekterte lymfeknuter.

Den vanligst brukte modaliteten for EBRT er fotonstråling (6MV), som blir generert i en lineærakselerator (linac) der flere mekaniske elementer brukes til å generere og forme fotonstrålen riktig. Ett av disse er flatteningfilteret, som brukes til å flate ut fluensprofilen til strålen. Dette filteret kan også fjernes, hvilket fører til at den kjegleformede profilen til fotonstrålen bevares, i en såkalt flatteningfilter-fri (FFF) stråle. EBRT med FFF stråler gis med høyere doserate (og muligens redusert behandlingstid) enn stråler med flatteningfilter, og kan brukes til behandling av flere kreftformer.

Dette masterprosjektet inkluderte 15 pasienter, som tidligere fikk strålebehandling for livmorhalskreft på St.Olavs Hospital, med EBRT, BT og sekvensiell EBRT boost av metastatiske lymfeknuter. I denne studien ble både standard 6MV VMAT og FFF VMAT doseplaner inkludert SIB laget retrospektivt for alle pasienter. Disse planene ble evaluert og sammenlignet med hensyn til hvorvidt disse kunne oppfylle definerte dosekrav, i tillegg til sammenligning av homogeniteten og konformiteten til planene. Alle planene ble videre levert til kvalitetssikringsfantom (QA fantom), for å vurdere hvor godt disse planene kunne leveres av en klinisk linac. Flere parametere ble tatt ut fra QA målingene, og 6MV og FFF planene ble videre sammenlignet med hensyn til disse. Målet var å undersøke hvorvidt FFF planer kunne leveres med samme presisjon

fra en klinisk linac, som de tilsvarende 6MV planene.

Både standard 6MV og FFF planer var tilfredsstillende med hensyn til dosedekning av målvolum, og de var omtrent like med hensyn til skjerming av nærliggende risikoorganer, når de ble evaluert et doseplanleggingssystem. Men, data fra QA målingene viste at 6MV doseplaner ble mer presist levert til QA fantomet, sammenlignet med de tilsvarende FFF doseplanene. For de komplekse og inhomogene målvolumene som skal bestråles i pasienter med livmorhalskreft med lymfeknutemetastaser, foretrekkes dermed standard 6MV VMAT SIB planer fremfor FFF planer.

Preface

This thesis presents my master project in Biophysics and Medical Technology at the Norwegian University of Science and Technology (NTNU). The work in this project was carried out during the spring semester of 2018, at the radiotherapy department at St. Olavs Hospital in Trondheim. I would like to thank my supervisors at St. Olavs Hospital, medical physicists Anne Beate Langeland Marthinsen and Josefine Ståhl Kornerup, for useful guidance, discussions and motivation during my work. I would also like to thank my fellow students and professors at the biophysics section at NTNU for helpful feedback and motivation, both during our weekly meetings and in everyday conversations. Thanks also to the head of the radiotherapy department, Anne Dybdahl Wanderås, for letting me write my master thesis at the department.

Even T. Andersen
Trondheim, June 2018

Contents

Abbreviations

3D MRI - 3-dimensional magnetic resonance imaging

BED - Biologically effective dose

BOT - Beam-on time

BT - Brachytherapy

CI - Conformity index

CTV - Clinical target volume

CT - Computed tomography

DD - Dose difference

DTA - Distance to agreement

$\mathbf{D}_{\boldsymbol{x}\ cm^3}$ - The minumum dose to the most irradiated x cm^3 of an organ at risk

$\mathbf{D}_{\boldsymbol{x}\ \%}$ - The minumum dose to the most irradiated x % of an organ at risk

EBRT - External beam radiotherapy

EMBRACE - European study on MRI-guided brachytherapy in locally advanced cervical cancer

EMBRACE II - Image guided intensity modulated external beam radiochemotherapy and MRI based adaptive brachytherapy in locally advanced cervical cancer

EQD2 - Biological equivalent dose in 2 Gy fractions

FDG-PET - Fluorodeoxyglucose-positron emission tomography

FF - Flattening filter

FFF - Flattening filter free

GEC-ESTRO - Groupe Européen de Curiétherapie and the European Society for radiotherapy & oncology

GTV - Gross tumor volume

GYN GEC-ESTRO - Gynaecological Groupe Européen de Curiethérapie (brachytherapy comittee) and the European Society for radiotherapy & oncology

HI - Homogeneity index

HPV - Human papillomavirus

IGABT - Image guided adaptive brachytherapy

IMRT - Intensity modulated radiotherapy

Linac - Linear accelerator

LN(s) - Lymph node(s)

LNM - Lymph node metastasis

MLC(s) - Multileaf collimator(s)

MU(s) - Monitor unit(s)

OAR(s) - Organ(s) at risk

PCI - Paddick conformity index

PTV - Planning target volume

PTV-E - Elective planning target volume

PTV-T - True pelvic planning target volume

QA - Quality assurance

RT - Radiotherapy

SBRT - Stereotactic body radiation therapy

SIB - Simultaneous integrated boost

VMAT - Volumetric modulated arc therapy

1 Introduction

Cervical cancer is the fourth most common cancer type for women worldwide [1]. In well developed countries, the survival rate is high, especially for early stage cancers. 90% of all cervical cancer deaths occur in less developed countries, where screening programs are not common [2]. From 2011 to 2015 there were on average 324 new incidences of cervical cancer per year in Norway [3]. This corresponds to 2.3% of all cancer diagnosis in this period. In the same four-year period, 70 women died as a cause of cervical cancer, corresponding to 1.4% of all cancer related deaths in Norway. Cervical cancer is associated with a certain risk of spreading of the cancer to nearby lymph nodes in the pelvic area. These so-called lymph node metastases can be found in about 45-47% of all cervical cancer patients. [4, 5], and are associated with reduced probability of long term survival [6].

Aside from surgery, cervical cancer is treated using radiotherapy. The common treatment of advanced staged cancer is to combine external beam radiotherapy (EBRT) with brachytherapy (BT) in addition to concomitant chemotherapy. Daily fractions of EBRT is commonly given for 4-5 weeks. BT is given as a radiation boost to the primary tumor region in the last few weeks of, or after, the EBRT treatment. For patients with lymph node metastases, external radiation boost is also given to the positive lymph nodes. This lymph node boost has traditionally been given sequentially, that is, after finishing the EBRT of the primary tumor in the pelvic area. However, modern treatment techniques such as intensity modulated radiotherapy (IMRT) and volumetric modulated arc therapy (VMAT) have made it easier to deliver this boost at the same time as the lower doses are delivered to the primary pelvic target. This is called simultaneous integrated boost (SIB).

In contrast to sequential boosting of positive lymph nodes, SIB has some potential advantages. Studies have indicated that SIB is a useful and feasible tool in radiotherapy, which provides favourable clinical outcomes regarding both reduction of the overall treatment time, local tumor control and acceptable normal tissue side effects,

both for cervical cancer [7] and other types of cancer [8, 9].

Flattening filters (FFs) are used in linear accelerators (linacs) to flatten the fluence profile in clinical photon radiation beams. Because a certain share of the photons are absorbed and scattered in the FF, the dose rate is reduced and the scattered dose is increased by the filter. The FF can also be removed to increase the dose rate and thereby decrease the delivery time [10, 11]. Less scattered radiation is also an advantage using flattening filter-free (FFF) beams.

In this master thesis, both standard 6MV VMAT and FFF VMAT plans with SIB have been retrospectively generated for 15 cervical cancer patients with lymph node metastases. First, 6MV and FFF treatment plans were generated in correspondence with current clinical standards, in order to assess any potential problems with respect to target volume dose coverage and sparing of nearby organs at risk (OARs). Second, all plans were delivered to a quality assurance (QA) phantom from a clinical linac. Several parameters were extracted from these measurements, in order to compare the accuracy in the treatment plan delivery for the FFF plans to that of the standard 6MV plans. The main aim was to study if FFF plans were as good as the standard 6MV plans for this type of cervical cancer treatment, and to assess the possibility of using this in the clinic.

2 Theory

2.1 Cervical cancer

2.1.1 The cervix

The cervix is located in the lower part of the uterus, connecting the inferior part of the uterus with the superior part of the vagina [12] (figure 1). The inner part of the cervix is called the endocervix. This part forms the endocervical canal from the vagina to the uterus and consists of glandular cells. The outer part of the cervix, facing the superior lumen of the vagina is called the ectocervix. This part consists of squamous cells.

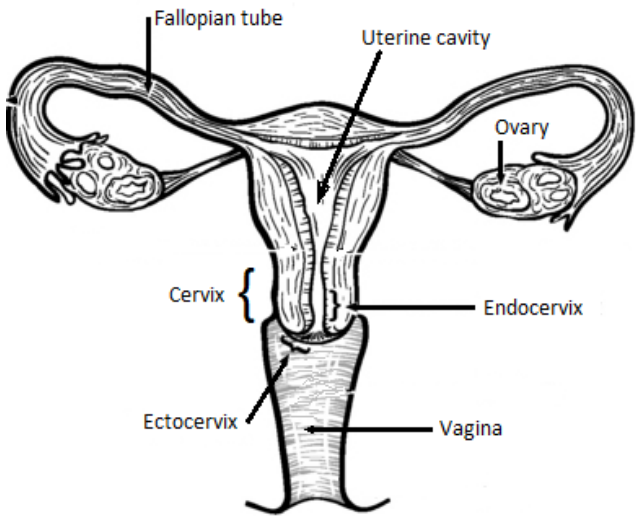

Figure 1: The anatomy of the female reproductive system. Adapted from [13].

Most cervical cancers develop from abnormal cell changes in the cervix. These changes are most likely to occur in the region where the ectocervix meets the endocervix, in the so-called "transformation zone" [14]. Most cervical cancers develop from changes in the squamous cells. In some cases, however, the cancerous changes occur in the glandular cells, so-called adenocarcinoma. The main cause of cervical cancer is an infection with a high risk type of the HPV [15]. There are over 100 different types of the HPV, but most of these are considered harmless. However, some of the HPV types are considered as high-risk types. Amongst them are HPV-16 and HPV-18, which on a worldwide basis contributes to 70% of all cervical cancers [16]. The types HPV-45

and HPV-31 contributes to another 10%.

2.1.2 Lymph node metastasis

The lymphatic system is a unidirectional circulatory network in the body. It consists of lymphatic vessels, lymph nodes and lymphatic organs which in total comprises the circulatory network. Among others, the lymphatic system has two main tasks. The first is to return interstitial excess fluid back into the blood stream from different body tissues. When the blood carries nutrients to different parts of the body, these nutrients will diffuse into the tissue from the blood capillaries, along with fluid from the blood. The excess fluid in the body tissue will then drain back into lymphatic capillaries. This fluid, consisting mainly of water and proteins, is called lymph. After entering the lymphatic capillaries, the lymph travels through the lymphatic system to re-enter the blood stream where the lymphatic vessels are connected to the subclavian vein. The other task of the lymphatic system is to contribute to the immune defence of the body. In the case of a viral or bacterial infection in a certain body tissue, the virus or bacteria will be brought through the lymphatic system by the lymph. Lymph nodes containing lymphocytes (white blood cells) will then cleanse this fluid of the foreign substances and try to eliminate them, so that the fluid that re-enters the blood stream is clean and healthy.

Cancer that originates in a body tissue can spread through the body, so called metastasis. This can occur if the tumor cells are able to invade either the cardiovascular system or the lymphatic system. In the case where tumor cells enters the lymphatic system, many cancer cells will be recognized as foreign by the lymphocytes and may be eliminated. However, in some cases cancerous cells may be able to settle in regional lymph nodes close to the primary tumor site. From here they may be able to proliferate, and new tumors may start growing. Lymph node metastases (LNM) can be important factors in the prognostics of the disease [17]. The first two paragraphs (of 2.1.2) are mainly based on [18] and [19].

LNM is also an important factor in the case of cervical cancer, where cancerous cells may spread from the primary tumor in the cervix to regional lymph nodes in the pelvic area (figure 2). The diagnosis of positive LNs (LNs with metastases) are in modern days primarily based on FDG-PET. This imaging technique is good for providing functional information, and so it enables the detection of positive lymph nodes even if the infected lymph node has not grown in size [5]. LNM are relatively common for cervical cancer patients. Studies have found that about 45-47% of cervical cancer patients are diagnosed with positive LNs [4, 5]. This fraction is increased with higher FIGO stage (see 2.1.3). Positive LNs may significantly affect the chances of survival. One study found that the five-year survival rate for patients with negative pelvic LNs (LNs without metastases) was 82.0% [6]. For positive pelvic LN the same survival rate was 55.1%.

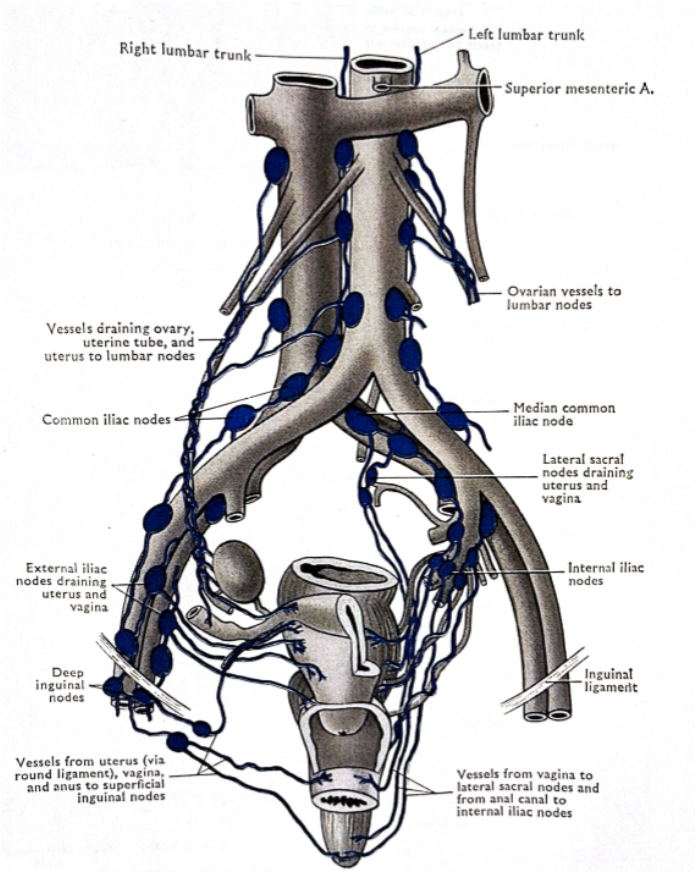

Figure 2: Diagram showing the lymph nodes in the female pelvic region. Adapted from [19].

2.1.3 FIGO system for staging of cervical cancer

In order to decide the adequate treatment regimen, it is essential to determine the extent of the tumor and possible spread of the cancer. Various diagnostic imaging techniques and examination methods can be used for this purpose. The process of correctly describing the disease is referred to as cancer staging. The FIGO (International Federation of Gynecology and Obstetrics) system is used to determine the cancer stage, depending on certain characteristics of the cancer [20]. According to the FIGO system, there are 4 main stages of the cervical cancer, each of them with additional sub-stages for thorough classification of the cancer. A short description of the classification of the different stages can be seen in table 1. The standard treatment regimen differs between FIGO stages [21]. For stages IA and IB radical hysterectomy with pelvic lymphadenectomy (surgery) is common. For advanced IB, however, radiotherapy (RT) with concomitant chemotherapy can be necessary. IIA, IIB, IIIA, IIIB and IVA are usually treated with EBRT and intracavitary RT. IVB is treated individually depending on age, general condition, tumor extension and localization. RT and chemotherapy are possible modalities.

Table 1: FIGO system for staging of cervical cancer[20]. This system describes the tumor extent for different stages of cervical cancer.

Stage		Description
I		Carcinoma strictly confined to the cervix.
	IA	Invasive carcinoma (5-7mm). Diagnosed only by microscopy.
	IB	Clinically visible lesion confined to the cervix.
II		Carcinoma invades beyond the uterus, but not to pelvic wall or to the lower third of the vagina.
	IIA	Without parametrial invasion.
	IIB	With obvious parametrial invasion.
III		Tumor extends to the pelvic wall and/or involves lower third of the vagina.
	IIIA	Tumor involves lower third of vagina, with no extension to pelvic wall.
	IIIB	Tumor extends to pelvic wall and/or causes hydronephrosis or nonfunctional kidney.
IV		Carcinoma extends beyond the true pelvis or has involved the mucosa of the bladder or rectum.
	IVA	Spread of the growth to adjacent organs.
	IVB	Spread to distant organs.

2.1.4 Cervical cancer statistics

According to GLOBOCAN, a project of the International Agency for Research on Cancer, there were about 528 000 new incidences of cervical cancer worldwide in 2012, in which about half of the incidences had a mortal outcome [2]. It is the fourth most common cancer for women in total, and the most common cancer type for women under 35 years of age. Both the incidence and mortality was highest in poorly developed countries.

In Norway, 342 new cases of cervical cancer were reported in 2016 [22]. In the period from 2007 to 2011 the five-year relative survival was 79.0%. In the next five year period from 2012 to 2016 the five-year relative survival increased to 80.5%. In addition to screening programs, vaccines against HPV are now available for young women in Norway. From November 2016, women born in 1991 and later is offered to take this HPV vaccine for free, an offer which stands for two years. According to the Norwegian Institute of Public Health it is estimated that about 83 000 women have taken the HPV vaccine in the first year of offer. Screening and vaccination might be an important contribution to the decrease of cervical cancer deaths. In countries where screening programs have been practiced for a long time, the rates of cervical cancer deaths have decreased by as much as 65% over the last four decades. In Norway, incidence rates for cervical cancer decreased from 18.7 per 100 000 in 1970 to 9.6 per 100 000 in 2011 [2].

2.2 Cervical cancer treatment

The treatment of cervical cancer is dependent on the cancer stage (see 2.1.3). For advanced cancer stages the tumor is likely to be harder to remove by surgery because of invasion of nearby tissue. Radiation therapy (RT) is then the common way of treatment, often in combination with chemotherapy. The goal of the radiotherapy is to deliver a high dose homogeneously to the tumor, while sparing the surrounding OARs. For cervical cancer with LN metastases the most commonly exposed OARs are the bladder, rectum, sigmoideum, bowel bag, kidneys and femoral heads. This can be seen in figures 3, 4 and 5.

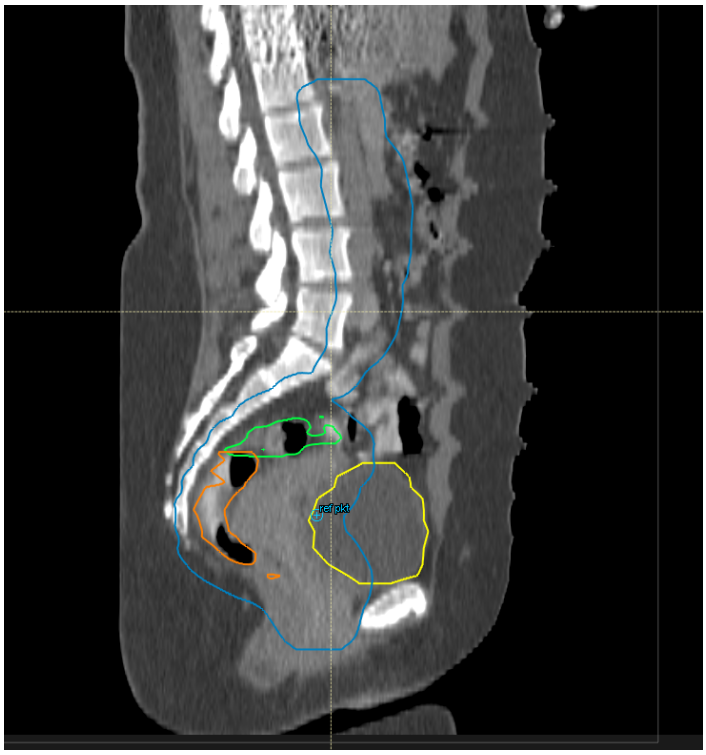

Figure 3: Sagittal plane CT view of a patient included in this study, along with delineated clinical structures. The blue structure is the combined planning target volume (PTV) for both main pelvic and elective targets (PTV-T + PTV-E). The green structure is the sigmoideum, the orange structure is the rectum (including the anal canal) and the yellow structure is the bladder. The image is taken from the RayStation treatment planning system.

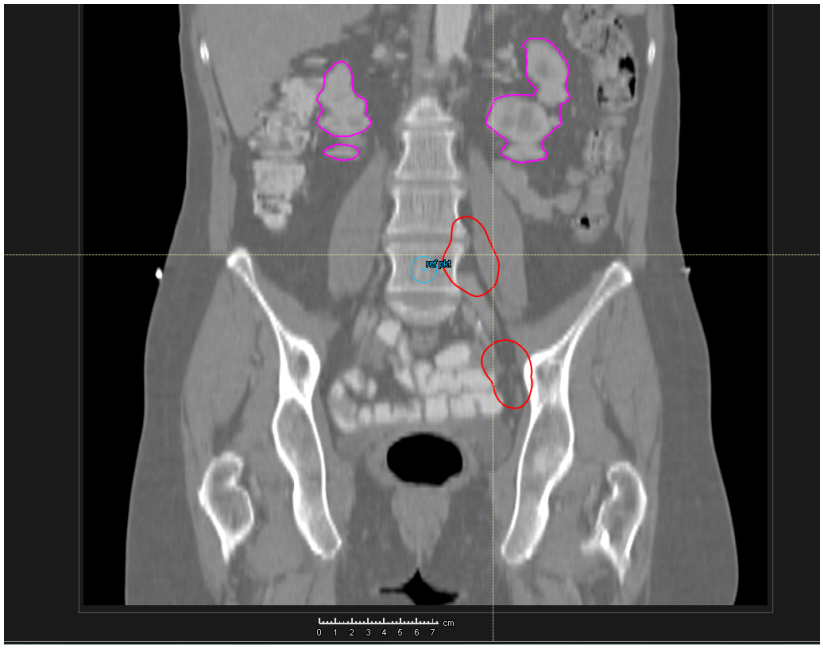

Figure 4: Coronal plane CT view of a patient included in this study, along with delineated clinical structures. The red structures are positive lymph node planning target volumes (PTVs). The pink structures are the kidneys. The image is taken from the RayStation treatment planning system.

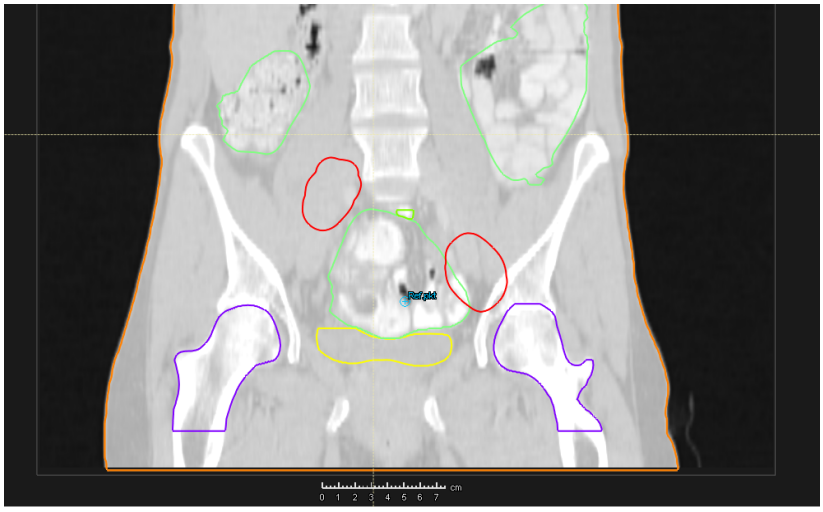

Figure 5: Coronal plane CT view of a patient included in this study, along with delineated clinical structures. The red structures are pathological lymph node planning target volumes (PTVs). The green structures are the bowel bag, the purple structures are the femoral heads and the yellow structure is the bladder. The image is taken from the RayStation treatment planning system.

The RT of cervical cancer is generally a combination of external beam radiotherapy (EBRT) and brachytherapy (BT). The RT is commonly fractionated, so that the total irradiation dose is given over a course of 4-5 weeks. BT fractions are given to boost the irradiation of the primary tumor towards the end of, or after, the EBRT. If there are pathological lymph nodes present, external boost is delivered to these volumes.

2.2.1 EMBRACE studies

Traditionally the treatment planning for the cervical cancer BT boost mainly considered the dose delivered to a gynecological point A in order to calculate the dose delivered to the tumor [23]. In 2005 the GYN GEC-ESTRO working group came up with new recommendations regarding the BT part of the treatment [24]. These recommendations included treatment planning based on delineation of target volumes and OARs in 3 dimensional magnetic resonance imaging (3D MRI).

In 2008, an international study on MRI-guided brachytherapy in locally advanced cervical cancer (EMBRACE) was initiated. The main aim was to study the clinical effect of MRI guided BT, as opposed to the traditional treatment. This study was a multicenter prospective observational study, where 26 treatment centers were involved. There were no constraints for OARs, and BT dose prescriptions were in correspondence with the traditions of each of the participating clinics. 1416 patients were included in this study, and 37 of these were patients at St.Olavs Hospital in Trondheim. The traditional treatment at St. Olavs Hospital at the time was to give 2 Gy$\times$25 = 50 Gy in EBRT, followed by a sequential external boost to positive LNs of 2 Gy$\times$(5-7) = 10-14 Gy, giving a total dose of 60-64 Gy to positive LNs. In addition, 4 BT treatments were given to each patient to boost the irradiation of the primary tumor. These were given in 6 Gy fractions, as long as the OARs did not exceed their respective dose constraints. For the most exposed OARs, the maximum D_{2cm^3} EQD2 (see 2.3.7) constraints for the bladder, rectum and sigmoideum were 90 Gy, 75 Gy and 75 Gy respectively, for EBRT and BT in total. D_{2cm^3} is the minimum dose received by the most irradiated 2cm^3 of the OAR.

The RetroEMBRACE study was a retrospective study, that was carried out in 12 institutions [25]. This study applied the recommendations from Gyn GEC-ESTRO, regarding target delineation and dose volume reporting. In addition to RetroEMBRACE, several articles have considered the results from the EMBRACE study. Mazeron et. al found that a $D_{2cm^3} \leq 65$ Gy and $D_{2cm^3} \geq 75$ Gy was associated with respectively less and more rectal morbidity [26]. Kirchheiner et-al found that decreasing the BT dose and keeping the EBRT dose at 45 Gy in 25 fractions would reduce the risk of vaginal stenosis [27]. Results from EMBRACE formed the basis of a new, ongoing study, EMBRACE II, which was started in 2016. One of the aims of the EMBRACE II study was to implement an overall dose prescription protocol to improve the local control and to reduce the morbidity. The study protocol also implements modern RT techniques with simultaneous integrated boost (SIB, see section 2.3.6) of positive LNs and chemotherapy, and is now considered as a "golden standard" for treatment of cervical cancer patients. The EMBRACE II protocol study states that institutional practice regarding LN boosting can be followed. However, it is recommended to deliver a total EBRT + BT dose of about 60 Gy EQD2 to positive LNs. For simultaneous integrated boosting of positive LNs, the dose prescriptions are dependent on the location of pathological LNs. In the EMBRACE II protocol, the LN targets are allocated in risk groups for lymphatic spread, along with indications for nodal targets [28]:

- Small pelvis EBRT in low risk patients
- Large pelvis EBRT in intermediate risk patients
- Large pelvis + para-aortic EBRT in high risk patients

Figure 6 shows a diagram for LN clinical target volumes (CTVs) based on the risk of lymph spread. Hereby, the region indicating low risk will be referred to as true pelvis. Intermediate and high risk regions will be referred to as outside true pelvis.

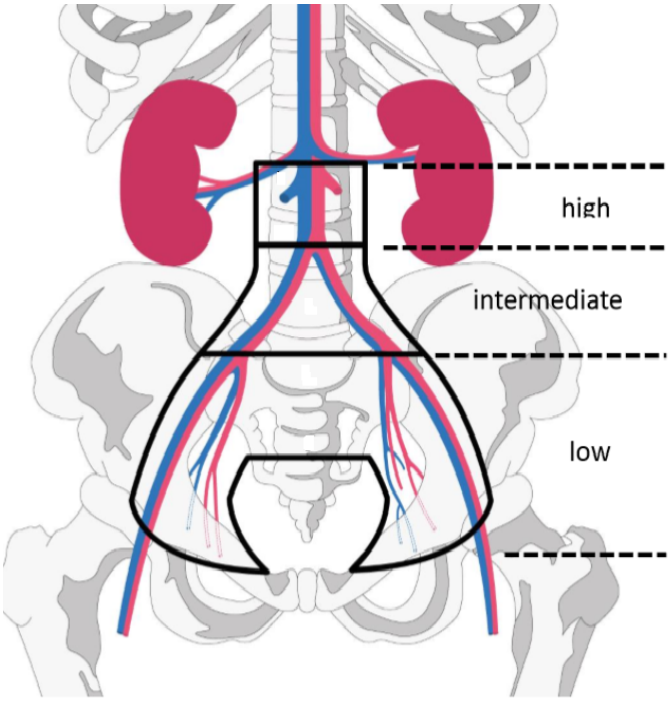

Figure 6: Diagram showing the regions of lymph node targets, based on risk of lymphatic spread. Taken from EMBRACE II study protocol [28].

Mohamed et. al assessed the doses to the LNs in the different risk regions, and found that positive LNs in the true pelvis received a non-negligible dose from the BT part of the treatment (3-4 Gy EQD2) [29]. Therefore, a prescribed dose of 25×2.2 Gy = 55 Gy to positive LNs within the true pelvis is recommended. Positive LNs outside the true pelvis should be prescribed 25×2.3 Gy = 57.5 Gy.

Several aspects from the EMBRACE II protocol are relevant to this project. The dose prescription standards have been altered from previous practice. For the EBRT part of the treatment, the standardized dose prescription is now 25 fractions of 1.8 Gy, in total 45 Gy. Earlier the total dose from EBRT was 50 Gy at many treatment institutions, among them St. Olavs Hospital. In addition, the SIB recommendations of 55 Gy and 57.5 Gy to positive LNs inside and outside the true pelvis respectively, are followed.

2.3 EBRT

EBRT is commonly used as treatment for cervical cancer, as well as most other solid tumors. EBRT includes several modalities (based on [30] and [31]): photon and electron beams are most commonly used, but proton and carbon beams are also used optionally.

2.3.1 Linear accelerator

Photon and electron beams are produced in a linear accelerator (linac). In a linac, electrons interacts with a microwave frequency electromagnetic (EM) field to accelerate through a waveguide. Towards the end of the waveguide the electrons reach a velocity close to the speed of light. The electrons themselves can be applied to the patient by scattering them to get a wide beam. If X-ray photons are to be applied, the electrons from the waveguide are directed onto a metal filament target with a high atomic number, usually tungsten. X-ray photons are then produced from the energy loss of the electrons, so-called bremsstrahlung. Energies of 6, 10, 15 or 18 MV are common for these photons. After generation the photons travel through a series of collimators and filters which are used to shape the beam. Further, multileaf collimators (MLCs) are used to shape the final radiation beam so that it fits the target volume to be irradiated. The MLC consists of several tungsten leaves of 0.5 - 1.0 cm in width, which can move independently and rapid to shape the beam. The gantry of the linac can rotate through 360 degrees enabling irradiation of the patient from any angle. This is an important feature in modern RT techniques, such as IMRT and VMAT (see 2.3.3).

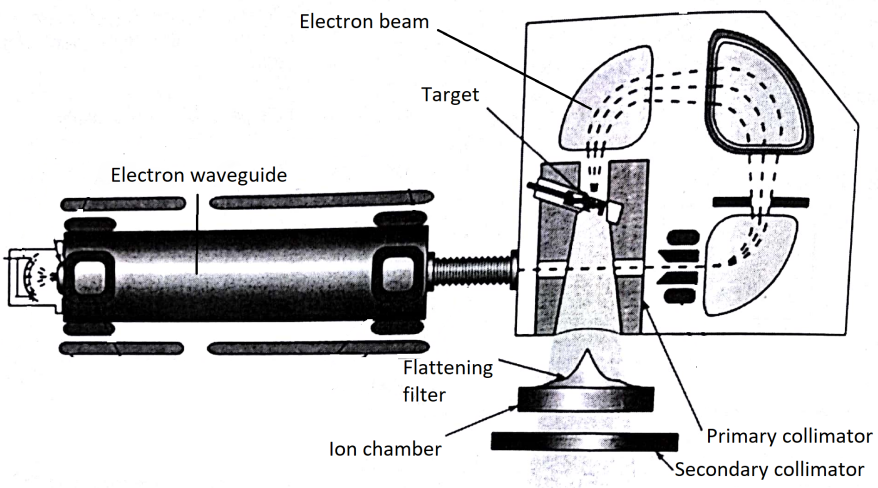

Figure 7: Working principle of the linac. Electrons travelling through the waveguide will be focused onto a metal target. Here, X-ray bremsstrahlung photons are produced. These photons travel through filters and collimators which are used to shape the beam. Adapted from [31].

2.3.2 Flattening filter

A filter used in the linac is the flattening filter (FF) (figure 7). Before reaching the FF, the bremsstrahlung photons are forward peaked, and therefore the fluence profile of the beam will be cone shaped [31]. Increased electron energy gives an increased peak of the dose distribution along the central axis of the x-ray beam. This is altered by the flattening filter, which is used to reduce the dose rate at the center of the beam, so that the beam profile is flattened (figure 8).

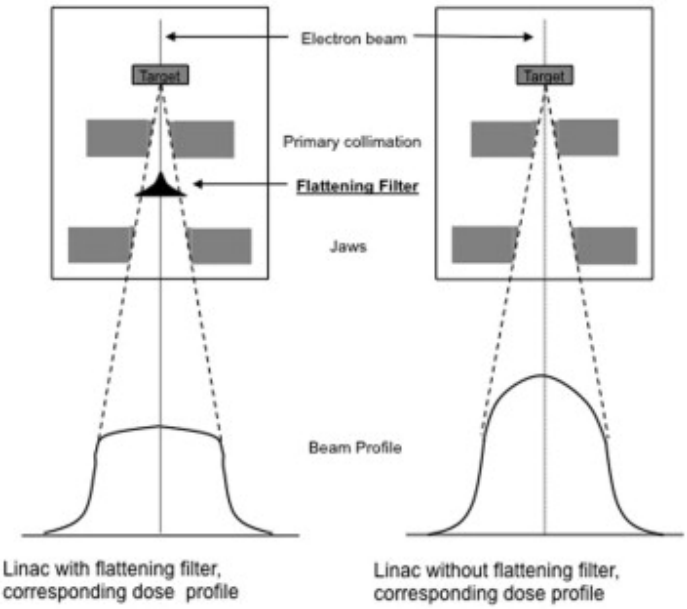

Figure 8: Fluence profiles of a photon beam with, and without, flattening filter. The filter is used to flatten the photon beam. When the filter is removed, the beam preserves its cone shaped form, with a peak towards the center of the beam. Taken from [32].

With modern treatment techniques and planning systems the FF is not a necessity, but it is useful for manually calculated treatment plans. Because the filter reduces the dose rate and increases the scattered dose, the inhomogeneity of the energy distribution across the treatment field will increase when using FF beams. EBRT treatment can also be performed without the use of flattening filter (FF). Removal of the FF will preserve the cone shaped fluence profile of the photon beams, which are hereby referred to as flattening filter-free (FFF) beams. FFF beams will have increased dose rates compared to FF beams, which can be advantageous in terms of delivery efficiency [10, 33]. This leads to shortening of the treatment delivery time, which is the main advantage of FFF beams. A significant reduction in treatment delivery time was found by both Aoki et al. [33] and Geng et al. [34], when using the FFF VMAT technique in stereotactic body radiotherapy (SBRT) of lung cancer. Aoki et al. found that the treatment time could be reduced by 50% or more. A significant reduction in treatment time was also found by Thomas et al. [10], for several cancer type treatments. However, in spite of increased treatment efficiency for FFF modes, this study expressed that this time reduction were unlikely to be of clinical value. Zhang et al., which studied FFF treatment of cervical

cancer patients that had undergone hysterectomy (surgical removal of the uterus), found that the FFF delivery time decreased with increasing energy [11]. At 6MV the delivery time was 11% less for FFF-VMAT plans compared to FF-VMAT plan, while at 10MV, the same reduction was 16%. Reduction of treatment time is favourable, both considering patient comfort and immobilization on the treatment table, and also for clinical reasons like limiting internal organ movement and possible filling of bladder and rectum during treatment. Otherwise, Zhang et al. found that the FFF beam achieved roughly the same target and organ at risk (OAR) dose distribution as the traditional FF beam. Kumar et al. found clinically acceptable plans for FFF rapid arc treatment plans for cervical cancer, but concluded that FF rapid arc treatment plans was more beneficial for cervical cancer, as the conformity and homogeneity was better with FF [35].

2.3.3 IMRT and VMAT

In conventional forward treatment planning, a set of beams are opposed to get a favourable dose distribution to satisfy the aim of delivering high tumor dose, and minimizing the normal tissue dose. However, it is difficult to decide if the calculated plan is the most optimal plan that could be contained. As it is a time consuming process to repeat all calculations for different opposing beams, inverse treatment planning techniques have now become a common treatment planning routine in most RT clinics. Inverse treatment planning includes an increased number of beam segments, and computerized optimization to satisfy the clinical aims. By specifying the desired dose distribution, the treatment planning system optimizes the result based on an objective function. In intensity modulated radiotherapy (IMRT) the prescribed dose is delivered to the target volume through a number of fixed beam segments [36]. Each beam segment is shaped by the MLC. Irradiation from several angles makes it possible to reduce the fluence in parts of the beam that irradiates critical tissues. This can be compensated for by increasing the fluence from other angles. This enables improved local tumor control and reduced normal tissue damage. Volumetric modulated arc therapy (VMAT) is a similar technique, where irradiation occurs during the gantry

rotation. The MLC leaves are continuously moving relative to each other, to shape the beam. Because of continuous irradiation, the treatment time is shorter for VMAT than for IMRT. The number of monitor units for VMAT is also less than for IMRT, leading to less scattered irradiation for the patient. However, VMAT is obviously more advanced than IMRT, and thus it requires more advanced treatment planning systems

2.3.4 Treatment process

3D CT images are the basis of all modern EBRT. These images give information about each individual patients anatomy, and enables the radiation to be given with a high level of precision. Physicians can delineate target volumes and clinical structures as the OARs directly into the images. By defining appropriate objectives and aims for the delineated structures, medical physicists and radiation therapists can then make EBRT treatment plans. This is done by using treatment planning software, where computerized algorithms calculates the doses in different regions in, and around, the target volumes. These techniques depends on a large number of parameters that can be adjusted to yield an optimal dose distribution. To reach the aim of high local tumor control and low normal tissue damage, computerized treatment planning optimization is a necessity for IMRT and VMAT. This way, each EBRT treatment plan is optimized for each individual patient before they receive their treatment. At the radiotherapy department at St. Olavs Hospital, RayStation treatment planning system (from RaySearch Laboratories AB, Sweden) is used for EBRT planning.

A relevant RayStation feature for this project is the dual arc configuration for VMAT treatment plans. This concept is an continuation from using two single arcs. The creation of two arcs involves several steps. First, an initial arc is generated. A fluence map is created for every 24 degrees of the rotation. For each of these fluence maps, two MLC openings will be formed. One is copied in the clockwise direction (2-4 degrees apart), and the other one in the counterclockwise direction. This is the starting point for the optimization. After one full rotation of this arc, another arc is

created in the opposite direction, in the same way as the first arc. These arcs will be quite similar if the collimator angle is the same for both arcs. However, if the collimator angle is different for each arc, the MLC openings will differ, and hence also the arcs. The dual arc configuration is somewhat different. For the initial arc 4 MLC openings are created for every 24 degrees. For each of thes control points the 4 MLC openings will be sorted into similar pairs which will be assigned to one arc each. The remaining optimization goes on as described for two single arcs. When creating dual arc, the collimator angle is the same for both arcs (counter-clockwise and clockwise). According to RayStation, this is often better than using single arcs if there is a region in between target volumes that requires reduced doses [37]. Compared to two single arcs, the dual arc configuration can produce arcs that creates less modulations and give better quality assurance results.

2.3.5 Monitor units

Monitor units (MU) are a measure of the linacs output. The actual output from the linac is measured as charges in the ionization chamber [31]. Therefore, for a certain beam energy, 100 MU is conventionally defined as the absorbed dose of 1 Gy in a water phantom under reference conditions [38]. MU is sometimes also referred to as "beam on time" (BOT). If the dose rate (MU/min) is constant, the number of MU will be propotional to the irradiation time. When using IMRT or VMAT the number of MUs will increase, since only parts of the target volume is irradiatied from each angle.

2.3.6 Simultaneous integrated boost

Additional radiation boost to positive lymph nodes has traditionally been given sequentially, that is, after the EBRT treatment of the main pelvic target. With modern treatment planning systems and IMRT and VMAT techniques (see 2.3.3) it is easier to deliver this boost at the same time as the main pelvic irradiation. This is called simultaneous integrated boost (SIB). Studies have shown that SIB has several advantages for cervical cancer treatment. Jen-Yu et. al investigated both IMRT- and VMAT-SIB techniques. Both techniques were found promising with respect to dose distribution

and tumor coverage in cervical cancer patients [39]. The rates of acute toxicity have also been found to be acceptable [40]. Feng et. al found that SIB IMRT showed a clear dosimetric advantage compared to IMRT with sequential boosting, a significant reduction of OAR doses and reduction of hot spots both in the pelvic area and OAR volumes [7]. Reduced overall treatment time is an advantage both for patients and for the treating institution. Clinical time and resources can be saved as the treatment only requires one treatment plan, making both treatment planning and delivery easier.

2.3.7 Biologically effective dose and equivalent dose

Absorbed dose is a measure of the energy absorbed per unit mass [41]. The doses given in radiotherapy are usually fractionated to utilize the fact that normal tissue cells have a higher repair capacity than tumor cells. When the total dose is split into several fractions, the biologically effective dose (BED) may differ from the actual total dose. Assuming n fractions of dose d, the BED can be written as:

$$BED = nd \cdot \Big(1 + \frac{d}{\alpha/\beta}\Big). \tag{1}$$

The α/β-ratio is the dose where the linear and quadratic components of the linear quadratic model are contributing equally to cell killing.
Since many fractionation regimens use a fractionation dose of 2 Gy, another common quantitation of the dose given is the EQD2. The EQD2 is the biological equivalent dose in 2 Gy fractions [41]. This is given by

$$EQD2 = \frac{BED}{\big[1 + \frac{2}{\alpha/\beta}\big]} = nd \cdot \frac{\big[d + (\alpha/\beta)\big]}{\big[2 + (\alpha/\beta)\big]}. \tag{2}$$

2.3.8 Homogeneity and conformity indices

An important aim of the EBRT is to deliver the dose homogeneously to the planning target volume (PTV). A way of quantifying the homogeneity of the dose distribution is the homogeneity index (HI) [35]. This index can be defined in several ways, but a common definition is:

$$HI = \frac{D_{5\%}}{D_{95\%}}, \tag{3}$$

where $D_{5\%}$ is the minimum dose received in 5% of the PTV that received highest dose, and $D_{95\%}$ is the minimum dose received in 95% of the PTV that received highest dose. With this definition, a HI = 1 is the optimal value, which implies perfect homogeneity of the dose distribution in the PTV. Increased HI implies poorer homogeneity.

Another index that is commonly used for measuring the quality of the dose distribution is the conformity index, which measures how well the distribution of dose matches the target volume. There are several definitions of this index as well. One is the Paddick conformity index (PCI) [42], which is defined as:

$$PCI = \frac{{TV_{PIV}}^2}{TV \times PIV}, \tag{4}$$

where TV is the target volume and PIV is the prescription isodose volume. TV_{PIV} is the volume of the TV lying within the prescription isodose (illustrated in figure 9).

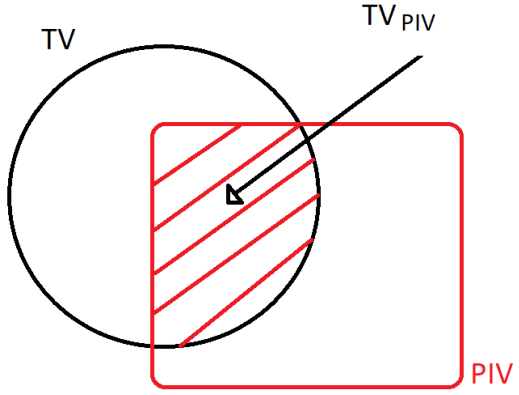

Figure 9: Illustration of the volumes used in calculating the PCI. TV is the target volume (black). PIV is the prescription isodose volume (red). TV_{PIV} volume of the TV lying within the PIV (red marked area). From these volumes the PCI can be found by equation 4.

The maximum possible TV_{PIV} volume is the smallest of the volumes TV and PIV. If the three volumes are equal, the volumes overlap each other perfectly, and the conformity of the dose distribution is perfect. This will give a PCI = 1. For dose distributions with poorer conformity, the PCI will decrease.

2.4 Quality assurance

In radiotherapy clinics quality assurance (QA) is an important procedure that ensures that each step in the treatment process is executed properly. QA is required for the individual treatment of patients including diagnostics, decisions regarding treatment, acquisition of anatomical data and treatment delivery. It is also required to ensure the equipment functions properly, as many errors can occur, both randomly and systematically. QA of linacs is done at daily, weekly and monthly bases, and mainly consists of radiation control and mechanical control. The radiation QA includes dose calibration measurements and ensuring that the photon beams are symmetric and properly aligned. The mechanical QA is to ensure that the geometry of the whole treatment system is satisfactory. Among other things, this includes isocentricity of both gantry and collimators, laser positioning and MLC control. The purpose of the QA is to ensure that the individual treatment of patients are in correspondence with what is planned.

Correct treatment delivery of VMAT plans is dependent on both dose rate, gantry speed and continuous shaping of the MLCs, making it a very complex process that requires high level of precision to be delivered safely and satisfactory. QA of VMAT is commonly done by delivering the radiation from a treatment plan to a phantom. The actual doses delivered at specific points are registered by the phantom, and the difference between the planned and the actual doses in the measured points can be calculated. Neither the treatment system nor the beam model is perfect, and so in practice there will be some differences between the planned and the delivered dose. To quantify this difference, there are two main parameters used:

◦ Dose difference (DD): difference between measured and calculated dose. A common requirement for acceptable delivery is that the DD should be less than 3% of the planned dose.

◦ Distance to agreement (DTA): Distance from the measurement point to the nearest point in the planned dose distribution that gets the same dose. A common requirement

for acceptable delivery is that the DTA should be less than 3mm.

The DD and DTA methods complement each other by being suitable for regions with low and high dose gradients respectively. However, because they are individually poor in certain regions, the so-called gamma method combines these two into one single measure called the gamma index [43]. At each measurement point, the combined DD and DTA passing criteria of less than 3% and 3mm respectively corresponds to a gamma index less than 1. The share of measurements points fulfilling these criteria are referred to as the gamma pass rate. At St. Olavs Hospital, the gamma pass rate should be at least 90% for a clinical acceptable plan.

2.5 Statistical analysis

The Wilcoxon signed rank test is a non-parametric test, closely related to the student's t-test. However, the Wilcoxon signed rank test has no assumptions of normality, as opposed to the t-test. This is appropriate when considering populations with a small number of samples. It is commonly used to analyze two related groups, where the samples are paired between the groups. The assumptions of the test is that the paired samples are independent from the other pairs in the data set, that the paired samples come from the same population, and that the data are measured on an intrinsically continuous scale. The null hypothesis of the Wilcoxon signed rank test is that the median difference between pairs of observations is zero. The alternative hypothesis is then that the median difference is not zero.

3 Materials and methods

3.1 Patients

15 cervical cancer patients with LN metastasis were included in this study. All patients previously received RT treatment at St. Olavs Hospital and were included in the EMBRACE study. At the time of treatment, these patients received 2 Gy×25 = 50 Gy from EBRT, followed by sequential boost of 2 Gy in 5-7 fractions, in addition to 4 BT fractions. For this master project all patient data was anonymized, and the patients were numbered 1 to 15. CT images for each patient were available through the RayStation (6R, v5.99.0.5) treatment planning system from RaySearch Laboratories AB, Sweden. The CT images included delineations of clinical structures, such as target volumes and OARs. These were delineated by physicians prior to the actual RT treatment. Before making retrospective treatment plans, the delineated structures were considered. A control of the existing structures and additional delineation of sigmoid colon and bowel bag were made by medical physicist at the department. In addition, auxiliary structures were delineated to improve the optimization of the dose distribution (see section 3.2).

3.2 Treatment planning

VMAT treatment plans, both standard 6MV and FFF, were made retrospectively for all 15 patients using RayStation. Prior to retrospective treatment planning, the delineated clinical structures were generally in correspondance with the EMBRACE II protocol [28] structures. The following lists are descriptions of the clinical and auxiliary structures used in this project, as well as the delineated OARs.

Target volumes:

- GTV-T: initial gross tumor volume of the primary cervix tumor.
- CTV-T: clinical target volume (GTV-T+suspected microscopic tumor extension).
- PTV-T: planning target volume. CTV-T + 12mm.

- CTV-E: clinical target volume in elective nodal region.
- PTV-E: planning target volume in elective nodal region.
- GTV-N(#): gross tumor volume of pathological lymph nodes.
- CTV-N(#): clinical target volume for pathological lymph nodes (GTV-N(#)+5mm).
- PTV-N(#): planning target volume for pathological lymph nodes (CTV-N(#)+8mm).

Auxiliary structures:

- GTV-T+10mm: a 10mm ring structure around GTV-T.
  To avoid hot spots in the OARs in the region that is likely to receive a non-negligible dose from BT.
- PTV_55Grad: 10mm ring structure around LN PTVs that were to receive 55 Gy.
  To achieve a dose fall off in the region around LN targets.
- PTV_55GradIN: The part of PTV_55Grad lying within PTV-T or PTV-E.
  To ensure that the dose is sufficiently high in this region.
- PTV_55GradOUT: The part of PTV_55Grad lying outside PTV-T and PTV-E.
  To achieve a dose fall off in the region around LN targets that is also outside PTV-T and PTV-E.
- PTV_57.5Grad: corresponding to the PTV_55Grad.
- PTV_57.5GradIN: corresponding to the PTV_55GradIN.
- PTV_57.5GradOUT: corresponding to the PTV_55GradOUT.
- PTV_45Help: The combined PTV-T and PTV-E minus the PTV-N(#) and its 10mm ring structure.
  To ensure that the dose in the PTV-T and PTV-E regions are kept at about 45 Gy.
- Spinal Canal PRV 3mm: 3mm ring (clinical practice) around spinal canal.
  A margin to ensure that the dose level is kept low in the region around the spinal canal.

OARs:

- Bladder
- Body

- Bowel bag
- Femoral heads
- Kidneys
- Rectum
- Sigmoideum (or Sigmoid)
- Spinal Canal

Figures 10 and 11 show some of the auxiliary structures used in this project.

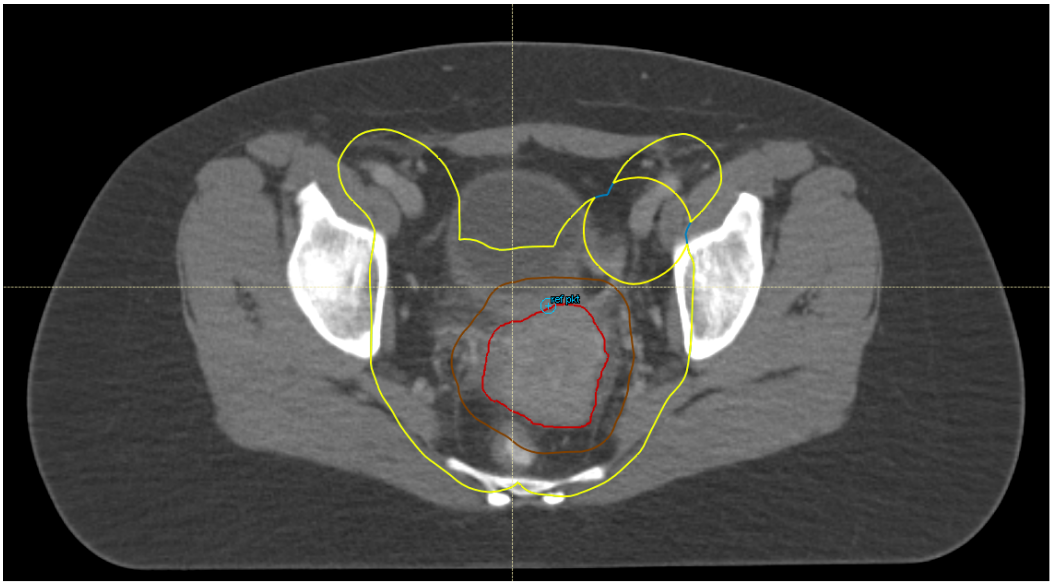

Figure 10: Image showing some of the auxiliary structures used in this project. The red structure is the "GTV-T" and the brown structure is the "GTV-T+10mm". The yellow structure is the "PTV_45Help". As seen there is a circular area to the right that is not covered by the "PTV_45Help" structure. This is a region with a LN target, a "PTV-N(#)", that is not supposed to overlap with "PTV_45Help". The image is taken from RayStation.

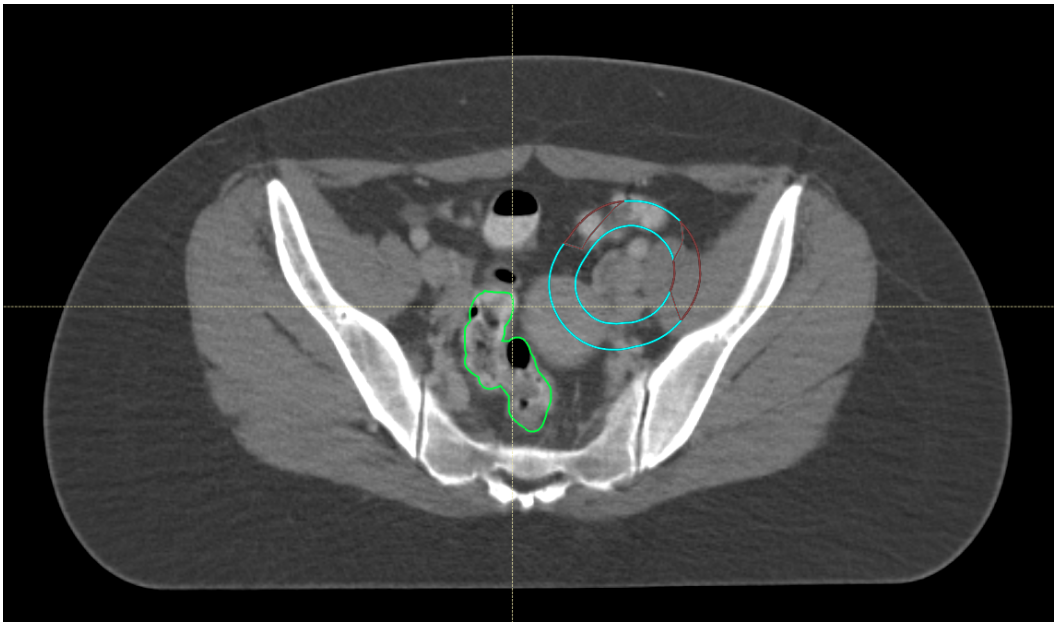

Figure 11: The blue structure is the "PTV_55GradIN" structure, and the brown structure is the "PTV_55GradOUT" structure. In total they make up the "PTV_55Grad". The green structure is the sigmoideum, and is included to illustrate the purpose of the "PTV_55Grad" structure, namely to achieve a dose fall off around the LN targets to avoid high doses to nearby OARs. The image is taken from RayStation.

Because of the clinical practice at St.Olavs Hospital, some structures that are included in the EMBRACE II protocol are not included in this project. These structures are mainly related to the BT part of the treatment, and are the following:

- CTV-T HR
- CTV-T LR
- ITV

3.2.1 Planning aims

The aim of the treatment plan optimization was to meet the dose constraints given by the EMBRACE II protocol [28]. In all plans the main priority was to fulfill the dose requirements for the target volumes (GTV, CTV and PTV). These are depicted in table 2. Positive LNs inside the true pelvis were prescribed 55 Gy, while positive

LNs outside the true pelvis were prescribed 57.5 Gy. The second priority was to fulfill the constraints for the OARs. These are depicted in table 3.

Table 2: Dose constraints for the target volumes as described in the EMBRACE II protocol [28]. ITV45 is also used in the protocol, but are not used in this project.

Target volume	Planning aims (%)	
PTV_45	$V_{95\%} > 95\%$	(42.75 Gy)
PTV-N(#)_55	$D_{98\%} > 90\%$ of prescribed LN dose	(49.50 Gy)
	$D_{max} < 107\%$ of prescribed LN dose	(58.85 Gy)
CTV-N(#)_55	$D_{98\%} > 100\%$ of prescribed LN dose	(55.00 Gy)
	$D_{50\%} > 102\%$ of prescribed LN dose	(56.10 Gy)
PTV-N(#)_57.5	$D_{98\%} > 90\%$ of prescribed LN dose	(51.75 Gy)
	$D_{max} < 107\%$ of prescribed LN dose	(61.53 Gy)
CTV-N(#)_57.5	$D_{98\%} > 100\%$ of prescribed LN dose	(57.50 Gy)
	$D_{50\%} > 102\%$ of prescribed LN dose	(58.65 Gy)

Table 3: Dose constraints for the OARs as described in the EMBRACE II protocol [28]. The two coloumns (LN 55 and LN 57.7) indicate if the LNs were to receive 55 Gy or 57.5 Gy. Structures as ovaries and duodenum are also described as optional OARs in the protocol, but are not included in this project. A CTV-HR+10mm is defined in the protocol, but is not used in this project. Instead GTV-T+10mm is used with a similar purpose, as described above.

OAR	Aims (LN 55)	Aims (LN 57.5)
Bladder	$D_{max} < 57.5$ Gy	$D_{max} < 60.4$ Gy
	$V_{40Gy} < 75\%$	$V_{40Gy} < 75\%$
	$V_{30Gy} < 85\%$	$V_{30Gy} < 85\%$
Body	$D_{max} < 58.9$ Gy	$D_{max} < 61.5$ Gy
Bowel bag	$D_{max} < 57.5$	$D_{max} < 57.5$
	$V_{40Gy} < 250$ cm^3	$V_{40Gy} < 250$ cm^3
	$V_{30Gy} < 500$ cm^3	$V_{30Gy} < 500$ cm^3
Femoral heads	$D_{max} < 50$ Gy	$D_{max} < 50$ Gy
GTV-T+10mm	$D_{max} < 46.4$ Gy	$D_{max} < 46.4$ Gy
Kidneys	$D_{mean} < 15$ Gy	$D_{mean} < 15$ Gy
Rectum	$D_{max} < 57.8$ Gy	$D_{max} < 60.4$ Gy
	$V_{40Gy} <85\%$	$V_{40Gy} <85\%$
	$V_{30Gy} <95\%$	$V_{30Gy} <95\%$
Sigmoid	$D_{max} < 57.5$ Gy	$D_{max} < 60.4$ Gy
Spinal Canal	$D_{max} < 50$ Gy	$D_{max} < 50$ Gy

3.2.2 Treatment plan optimization

To meet the dose requirements for both the target volumes and the OARs, the dose objectives for each structure were assigned different weights according to the priority of the structure. Target volume structures were prioritized before OAR structures, and hence they were assigned higher relative weights. In cases where the optimization were unable to fulfill the dose requirements initially, these objective weights could be adjusted to improve the optimization and possibly meet the requirements. Figures 12

and 13 shows the objectives used for the optimization in a patient with positive LNs inside and outside the true pelvis respectively.

Bladder	Dose Fall-Off [H]45.00 Gy [L]10.00 Gy, Low dose distance 3.00 cm
Bladder	Max DVH 30.00 Gy to 85% volume
Bladder	Max DVH 40.00 Gy to 75% volume
Bladder	Max Dose 57.80 Gy
Body	Max Dose 58.90 Gy
Body	Dose Fall-Off [H]45.00 Gy [L]20.00 Gy, Low dose distance 6.00 cm
Bowel bag	Dose Fall-Off [H]45.00 Gy [L]15.00 Gy, Low dose distance 4.00 cm
Bowel bag	Max Dose 57.50 Gy
Bowel bag	Max DVH 40.00 Gy to 34% volume
Bowel bag	Max DVH 30.00 Gy to 68% volume
CTV_45union	Min EUD 45.00 Gy, Parameter A 1
CTV-N_55union	Min Dose 55.30 Gy
CTV-N_55union	Min DVH 56.10 Gy to 50% volume
FemoralHead (Left)	Max Dose 50.00 Gy
FemoralHead (Right)	Max Dose 50.00 Gy
GTV-T+10mm	Max Dose 46.35 Gy
Kidney (Left)	Max EUD 10.00 Gy, Parameter A 1
Kidney (Right)	Max EUD 10.00 Gy, Parameter A 1
PTV_45Help	Min Dose 44.50 Gy
PTV_45Help	Max Dose 46.50 Gy
PTV_45union	Min DVH 42.75 Gy to 95% volume
PTV_55GradIN	Max Dose 55.00 Gy
PTV_55GradIN	Min Dose 45.00 Gy
PTV_55GradIN	Max DVH 50.00 Gy to 15% volume
PTV_55GradOUT	Dose Fall-Off [H]55.00 Gy [L]20.00 Gy, Low dose distance 5.00 cm
PTV-N_55union	Min Dose 50.00 Gy
PTV-N_55union	Max Dose 58.50 Gy
Rectum	Dose Fall-Off [H]45.00 Gy [L]15.00 Gy, Low dose distance 5.00 cm
Rectum	Max Dose 57.80 Gy
Rectum	Max DVH 40.00 Gy to 85% volume
Rectum	Max DVH 30.00 Gy to 95% volume
Sigmoid	Max Dose 57.80 Gy
Sigmoid	Dose Fall-Off [H]45.00 Gy [L]10.00 Gy, Low dose distance 5.00 cm
Spinal Canal	Max Dose 48.00 Gy
Spinal Canal PRV 3mm	Max Dose 50.00 Gy

Figure 12: A list of objectives used for the treatment planning optimization. These are the objectives used for a patient with LN targets to receive both 55 Gy only. The image is taken from RayStation.

Bladder	Dose Fall-Off [H]45.00 Gy [L]10.00 Gy, Low dose distance 3.00 cm
Bladder	Max DVH 30.00 Gy to 85% volume
Bladder	Max DVH 40.00 Gy to 75% volume
Bladder	Max Dose 60.40 Gy
Body	Max Dose 61.50 Gy
Body	Dose Fall-Off [H]45.00 Gy [L]20.00 Gy, Low dose distance 4.00 cm
Bowel bag	Max Dose 57.50 Gy
Bowel bag	Max DVH 40.00 Gy to 12% volume
Bowel bag	Max DVH 30.00 Gy to 25% volume
Bowel bag	Dose Fall-Off [H]45.00 Gy [L]15.00 Gy, Low dose distance 4.00 cm
CTV_45union	Min EUD 45.00 Gy, Parameter A 1
CTV-N_55union	Min Dose 55.30 Gy
CTV-N_55union	Min DVH 56.10 Gy to 50% volume
CTV-N_57.5union	Min Dose 57.70 Gy
CTV-N_57.5union	Min DVH 58.80 Gy to 50% volume
FemoralHead (Left)	Max Dose 50.00 Gy
FemoralHead (Right)	Max Dose 50.00 Gy
GTV-T+10mm	Max Dose 46.35 Gy
Kidney (Left)	Max EUD 10.00 Gy, Parameter A 1
Kidney (Right)	Max EUD 10.00 Gy, Parameter A 1
PTV_45Help	Min Dose 44.50 Gy
PTV_45Help	Max Dose 46.50 Gy
PTV_45union	Min DVH 42.75 Gy to 95% volume
PTV_55GradIN	Max Dose 55.00 Gy
PTV_55GradIN	Min Dose 45.00 Gy
PTV_55GradIN	Max DVH 50.00 Gy to 15% volume
PTV_55GradOUT	Dose Fall-Off [H]55.00 Gy [L]20.00 Gy, Low dose distance 5.00 cm
PTV_57.5GradIN	Max Dose 57.50 Gy
PTV_57.5GradIN	Max DVH 57.50 Gy to 12% volume
PTV_57.5GradIN	Min Dose 45.00 Gy
PTV_57.5GradOUT	Dose Fall-Off [H]57.50 Gy [L]30.00 Gy, Low dose distance 5.00 cm
PTV-N_55union	Min Dose 50.00 Gy
PTV-N_55union	Max Dose 58.50 Gy
PTV-N_57.5union	Min Dose 52.00 Gy
PTV-N_57.5union	Max Dose 61.50 Gy
Rectum	Dose Fall-Off [H]45.00 Gy [L]15.00 Gy, Low dose distance 5.00 cm
Rectum	Max DVH 40.00 Gy to 85% volume
Rectum	Max DVH 30.00 Gy to 95% volume
Rectum	Max Dose 60.40 Gy
Sigmoid	Max Dose 60.40 Gy
Spinal Canal	Max Dose 48.00 Gy
Spinal Canal PRV 3mm	Max Dose 50.00 Gy

Figure 13: A list of objectives used for the treatment planning optimization. These are the objectives used for a patient with LN targets to receive both 55 Gy and 57.5 Gy. The image is taken from RayStation.

Further, all plans were made applying the following RayStation settings (except where noted):

- Dual arc.
- Energy: 6MV
- Optimization tolerance: 1.000E-7
- Iterations before conversion: 7
- Iterations: 120
- Leaf motion constraint: 0.5 cm/deg
- Treatment machine: Agility Trh [03 May 2016; 15:49:34 (hr:min:sec)] (6MV)
- Treatment machine: Agility Trh FFF [20 Oct 2015; 13:18:05 (hr:min:sec)] (FFF)

With the dual arc setting, the treatment plans are delivered with 2 arcs. For the 6MV plans these are called arc1 and arc2, which is usual convention in clinical practice at St.Olavs Hospital. For the FFF plans the arcs are called arc3 and arc4. This means arc1 in a 6MV plan corresponds to arc3 in a FFF plan, and arc2 corresponds to arc4.

3.3 QA measurements

QA measurements were performed by delivering all plans to a Delta^{4PT} phantom (from ScandiDos AB, Sweden). The phantom consists of two perpendicular detector plates of 200mm×200mm. These measurements took place at the radiotherapy department at St. Olavs Hospital. All measurements were done in one day, at one linac and with the same phantom setup, so that the conditions and equipment setup were equal for every treatment plan delivery. Figure 14 shows an image of the setup used. The data collected from the measurements were recorded in, and could be directly collected from, the software ScandiDos Delta 4 (Delta4, version 2014, 2014 ScandiDos AB©, Uppsala, Sweden).

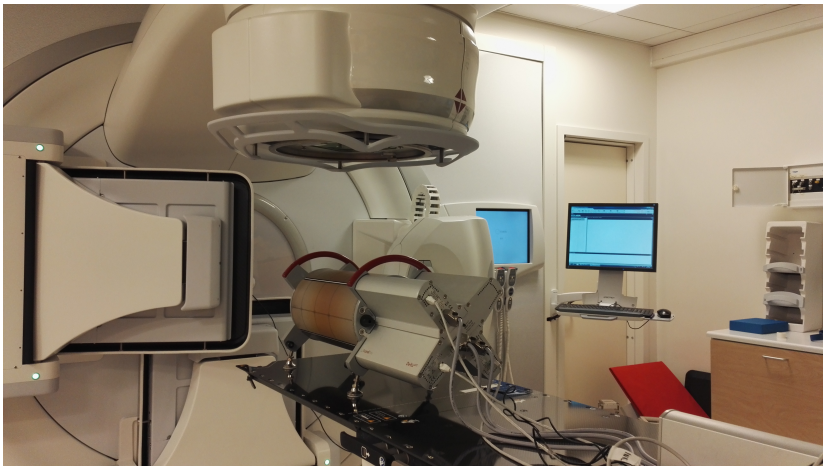

Figure 14: Picture of the setup, at the day of the QA measurements. The phantom is placed on the patient treatment couch, guided by lasers to ensure correct geometrical positioning. Treatment plans were delivered to the phantom from the linac, and measurement data were passed on from the phantom to the software.

In addition, the delivery times for each plan were measured manually using a stopwatch. Estimated delivery times for each plan were collected from RayStation for comparison. The volumes of the delineated PTVs (PTV-T, PTV-E and PTV-N(#)s) were extracted from RayStation. These were used to examine if the size of PTV volumes affected the delivery of the 6MV and FFF treatment plans. Both the total PTV volume and the relative boost PTV volume were used for this assessment. The total PTV volume is the sum of PTV-T, PTV-E and all PTV-N(#)s. The relative boost PTV volume was calculated as the volume of all PTV-N(#)s divided by the total PTV volume.

3.4 Treatment plan evaluation

The treatment plans, both standard 6MV and FFF, were evaluated in two steps. First, each plan were evaluated with regards to whether or not they fulfilled the dose constraints from the EMBRACE II protocol (tables 2 and 3), in addition to HIs and PCIs. Second, the treatment plans were compared with respect to QA measurement parameters.

HIs were calculated for each plan, as described by equation 3. These were calculated by extracting the $D_{5\%}$ and $D_{95\%}$ in the PTV_45Help structures, from the RayStation treatment plans. A high level of homogeneity is wanted in the region within PTV_45Help, as opposed to the positive LN regions. Therefore, the LN regions were excluded in this calculation.

PCIs were calculated, as described by equation 4, in 3 regions. One within the PTV_45Help structure, using PIV = 45 Gy isodose volume, and TV = PTV_45Help. Another PCI was calculated for the LNs to receive 55 Gy, using PIV = 55 isodose volume, and TV = all CTV-N(#)55 combined. For patients with positive LNs to receive 57.5 Gy, PCIs were calculated in these regions as well, using PIV = 57.5 isodose volume, and TV = all CTV-N(#)57.5 combined. The PCIs in the different regions are hereby referred to as PCI_{45}, PCI_{55} and $PCI_{57.5}$.

Based on both the treatment planning optimization and the QA measurements, the following parameters were used for comparison of 6MV and FFF plans:

- Target volumes satisfying dose constraint
- OARs not satisfying dose constraints
- HIs
- PCIs
- Gamma pass rates
- MUs
- Delivery times
- PTV volume effect

3.5 Statistical analysis

The subsequent extraction of the dose distributions to target volumes and OARs was carried out using the commercial software package MATLAB R2017a (The MathWorks, Inc., Natick, Massachusetts US. MATLAB R2017b, 2017). This software was used for

calculations and plotting of the results.

Because of a small number of samples (15 patients), the Wilcoxon signed rank test was used for statistical analyses of the 6MV plans versus FFF plans, with respect to the mentioned parameters. The test was conducted using the inbuilt MATLAB function signrank(). This function uses a default significance level of 5%, which is a commonly used significance level. In addition, MATLAB returns the exact p-value and not the asymptotic p-value, which is appropriate when considering a small number of paired samples. In addition to standard MATLAB plotting functions, trend lines were calculated and plotted using the polyfit() and polyval() functions. The MATLAB codes can be found in appendix B.

4 Results

The 15 patients included in this study had different numbers of positive LNs. The localization of these LNs also differed from patient to patient. Every patient had between 1 and 4 positive LNs inside the true pelvis, while 4 patients had positive LNs outside the true pelvis. The total PTV volumes, both for the pelvic and elective primary target, and the boost PTV volumes, were found from RayStation. These are depicted in table 4.

Table 4: Characteristics of the pathology of the 15 patients included in this study. The positive LNs in the true pelvis were to receive 55 Gy, and the LNs outside the true pelvis were to receive 57.5 Gy in total. The PTV volume is the sum of the PTV-T volume and the PTV-E volume (boost PTV volumes not included). The boost PTV volume is the sum of all PTV boost volumes for the patient in question.

Patient	**# of LNs in true pelvis**	**# of LNs outside true pelvis**	**PTV volume [cm^3]**	**Total boost PTV volume [cm^3]**	**FIGO stage**
1	2	-	2011.54	119.37	IIB
2	3	-	1787.56	116.94	IIA
3	1	-	1957.08	41.10	IIB
4	4	1	2209.12	193.67	IB
5	2	-	2212.24	90.82	IIB
6	1	-	1426.20	31.24	IIB
7	3	1	2546.02	140.69	IIB
8	1	2	1967.47	107.32	IIB
9	2	-	2002.40	89.76	IIIB
10	2	-	1741.75	83.20	IIB
11	5	-	2193.84	153.45	IIIB
12	2	-	1828.56	80.66	IIIB
13	2	-	1040.70	57.13	IB
14	1	1	2023.31	80.42	IIB
15	3	-	1610.81	90.37	IB

4.1 Treatment plan evaluation

All standard 6MV plans and all FFF plans were able to meet the dose constraints for the primary as well as for the LN target volumes. However, this lead to some difficulties in meeting the dose requirements for some OARs and help structures. The GTV-T + 10mm structure could not fulfill the constraints in any of the 30 plans. The dose volume constraints for rectum and bowel bag were also hard to meet in several plans. Figure 15 shows the different OAR constraints that could not be fulfilled, and the corresponding frequency (number of patients where the constraints could not be fulfilled). The maximum dose constraints for the bladder, body and sigmoid were met in all plans. An overview over which constraints that were exceeded for each patient can be found in appendix A (tables A3-A8).

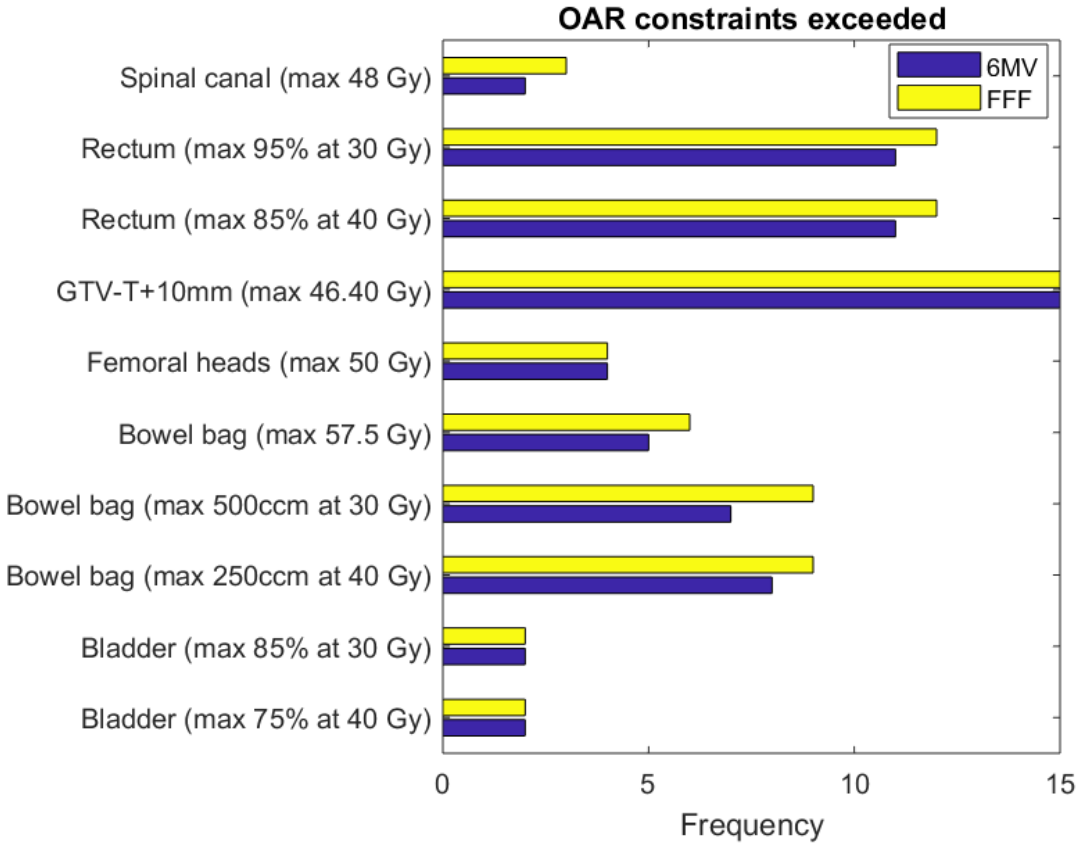

Figure 15: Bar chart showing the frequency of different OARs that could not fulfill the dose contraints. The constraints are indicated within parenthesis after the OAR name. The frequency is the number of patients in which the OAR dose constraints were exceeded. The bar graph is made in MATLAB.

To evaluate the clinical impact of the OARs exceeding dose constraints, it was investigated by how much the different OARs and help structures exceeded the constraints, both for the standard 6MV and FFF plans. The absolute exceedings, measured in Gy, are depicted in figure 16. For the dose volume constraints, the absolute exceeding indicates how many additional Gy were recorded at the partial volume. The 95% volume of the rectum exceeded its limit the most, with more than 7 Gy additional in median to this volume. Most other constraints were exceeded with less than 5 Gy in median.

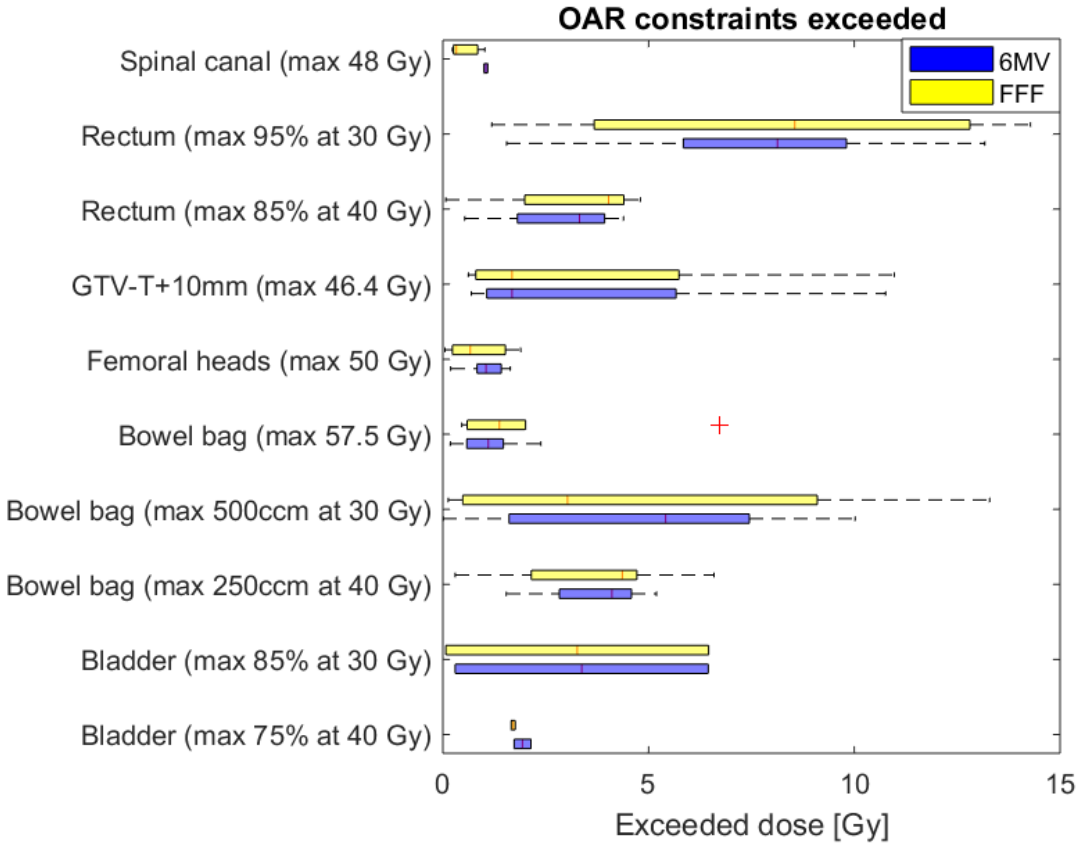

Figure 16: Box plot showing how much the OARs/structures exceeded their respective dose constraints in Gy, for both 6MV and FFF plans. The dose constraints are indicated in parenthesis after the name of each OAR/structure. The red line is the median value. The right and left edges of the boxes indicates the 75th and 25th percentiles respectively. The black whiskers extends to the most extreme data points. The red + mark is a possible outlier. The box plot is made in MATLAB.

For the dose volume constraints, figures 17 and 18 depict the exceedings for the OARs in percent and cm^3 respectively. In figure 17 it is indicated how many additional

percent of the volume lying within the given dose level. The rectum dose constraints were exceeded the most, and in some cases 100% of the rectum volume lied at the 30 Gy and 40 Gy dose level. The bladder constraints were not exceeded as much as the rectum constraints, and the 30 Gy and 40 Gy dose levels never covered the entire bladder volume. In figure 18 it is indicated how many additional cubic centimeters were lying within the given dose level. A large part of the bowel bag volume was often lying within the 30 Gy dose level. In extreme cases, more than 500 additional cubic centimeters were recorded at this dose level in FFF plans. At the 40 Gy dose level, the exceeding volumes were in general smaller.

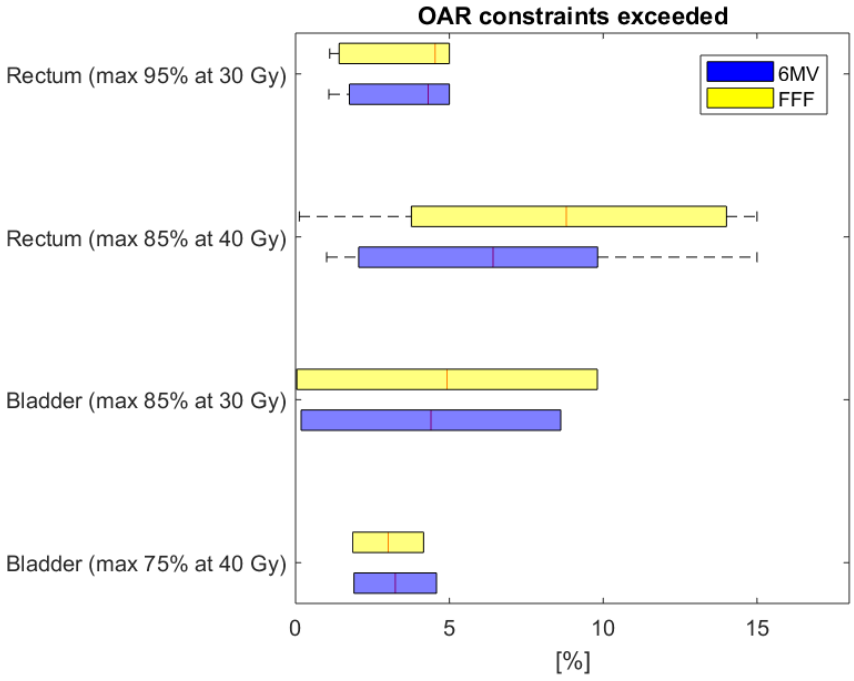

Figure 17: Box plot showing how much each of the OARs exceeded their dose volume constraints in percent. The exceeded percentage indicated is the absolute exceeding. The red line is the median value. The right and left edges of the boxes indicates the 75th and 25th percentiles respectively. The black whiskers extends to the most extreme data points. The box plot is made in MATLAB.

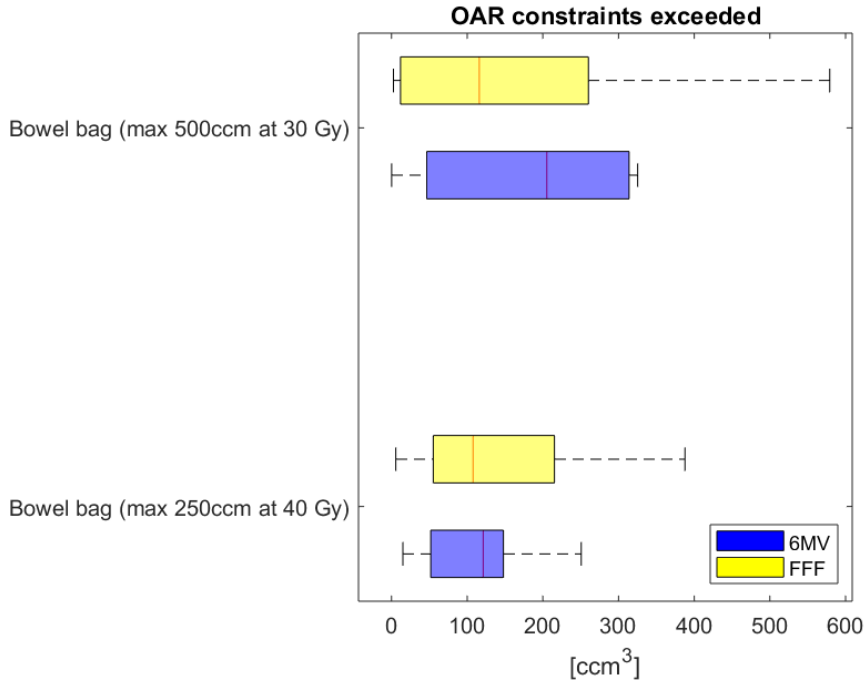

Figure 18: Box plot showing how much each the bowel bag structures exceeded the dose volume constraint. The plot indicates how many additional cubic centimeters were lying within the 30 Gy and 40 Gy isodose respectively. The red line is the median value. The right and left edges of the boxes indicates the 75th and 25th percentiles respectively. The black whiskers extends to the most extreme data points. The box plot is made in MATLAB.

The HIs for the 6MV and FFF plans were calculated as described by equation 3. The mean and standard deviation for 6MV and FFF are shown in table 5. HI for each plan can be found in appendix A (table A1). Statistical analysis of the HIs for 6MV and FFF plans, returned p = 0.02, meaning that the HIs were significantly different. As the mean HI for the 6MV plans was lower than that for FFF plans, this implies that the 6MV plans were more homogeneous.

Table 5: The mean HIs of the 6MV and FFF plans, including the standard deviation. The HIs for 6MV and FFF plans were significantly different (p = 0.02).

	6MV	FFF
Mean	1.071	1.076
Std	0.012	0.015

The PCIs for the 6MV and FFF plans were calculated as described by equation 4. The mean and standard deviation PCI_{45}, PCI_{55} and $PCI_{57.5}$, for both 6MV and FFF plans, are shown in table 6. PCI values for each plan can be found in appendix A (table A2). Statistical analysis of PCIs for 6MV and FFF plans compared, returned p = 0.60, p = 0.85 and p = 0.13 for PCI_{45}, PCI_{55} and $PCI_{57.5}$ respectively. This means that none of the PCIs were significantly different for 6MV versus FFF plans.

Table 6: The mean PCIs for the 6MV and FFF plans, including the standard deviation. PCI_{45}, PCI_{55} and $PCI_{57.5}$ indicate the regions where the PCIs are calculated, as described in section 3.4.

	6MV			FFF		
	PCI_{45}	PCI_{55}	$PCI_{57.5}$	PCI_{45}	PCI_{55}	$PCI_{57.5}$
Mean	0.70	0.53	0.72	0.69	0.52	0.66
Std	0.04	0.05	0.17	0.06	0.07	0.15

4.2 QA measurements

From the QA measurements, several parameters were extracted to compare the 6MV and the FFF plan deliveries. These are presented in the following sections.

4.2.1 Gamma pass rates

The gamma pass rate was analyzed for separate arcs as well as for the total plans. The results are depicted in figure 19 and table 7. Gamma pass rates for each individual patient can be found in appendix A (table A9). The total pass rate was higher for the 6MV plans than for the FFF plans in all but one patient (patient 12). This result was significant, with $p = 1.8 \cdot 10^{-4}$.

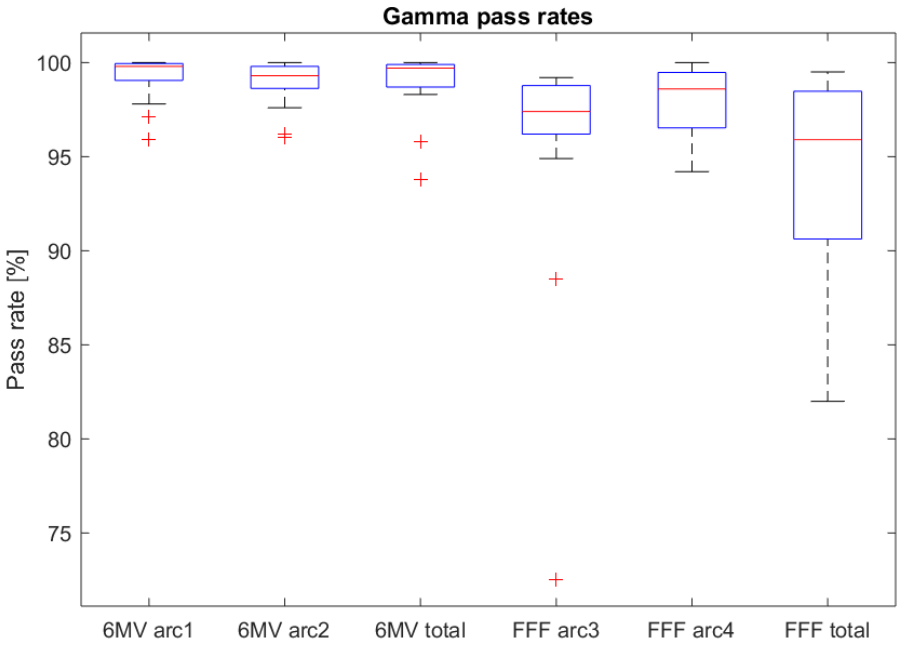

Figure 19: Boxplots of the passrates of both 6MV and FFF plans. The red line is the median value. The upper and lower blue edges of the boxes indicates the 75th and 25th percentiles respectively. The black whiskers extends to the most extreme data points, while the red + marks are possible outliers. The boxplot is made in MATLAB.

Table 7: The mean and standard deviations of the gamma pass rate measurements for both 6MV and FFF plans.

	6MV			FFF		
	arc1 [%]	arc2 [%]	Total [%]	arc3 [%]	arc4 [%]	Total [%]
Mean	99.1	98.8	98.9	95.4	97.9	94.3
Std	1.2	1.3	1.8	6.9	1.9	4.9

Figure 20 shows a pairwise comparison of the gamma pass rates of the the two different plans for all patients. All the 6MV plans, and 11 of 15 FFF plans, were delivered with a gamma passing rate greater than 90%.

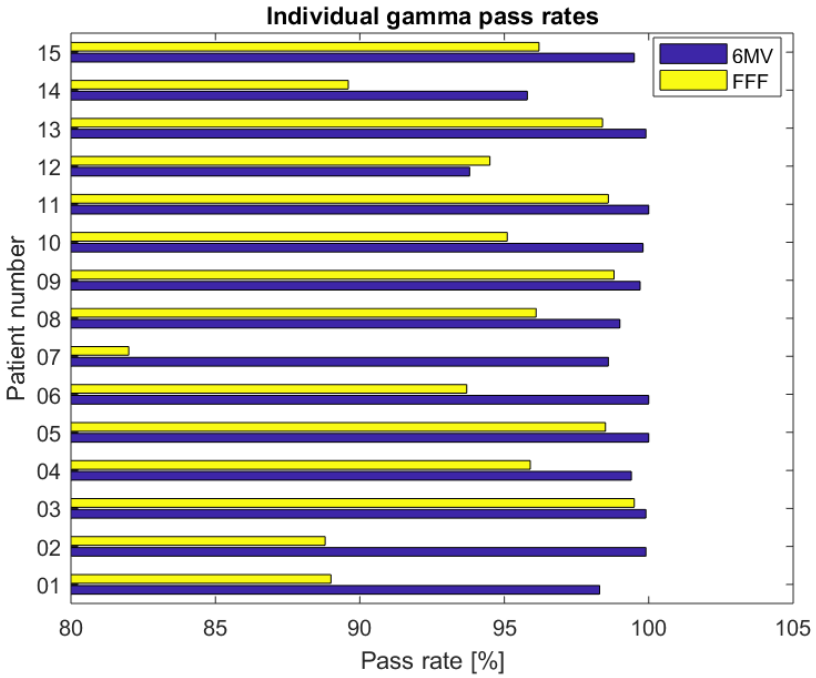

Figure 20: Bar chart showing the total gamma pass rates of both 6MV and FFF plans. The bar chart is made in MATLAB.

4.2.2 MUs

The total number of MUs were significantly greater for all the FFF plans ($p = 6.1 \cdot 10^{-5}$). The box plot in figure 21 shows the median total number of MUs for the 6MV and the FFF plans. The scatter plot in figure 22 shows the total number of MUs in 6MV plans vs FFF plans, for each individual patient.

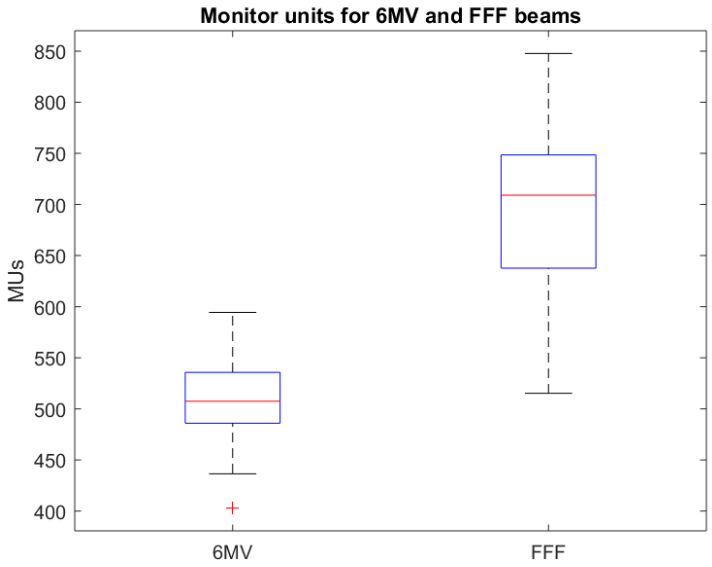

Figure 21: Boxplots of the total MUs for both 6MV and FFF plans. The red line is the median value. The upper and lower edges of the boxes indicates the 75th and 25th percentiles respectively. The black whiskers extends to the most extreme data points, while the red + marks are possible outliers. The boxplot is made in MATLAB.

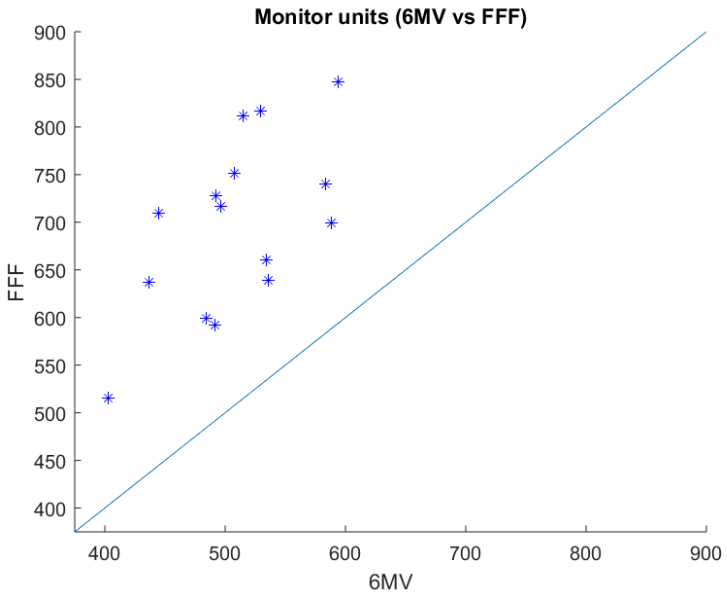

Figure 22: Scatter plot showing the total MUs for the 6MV versus the FFF plans. The blue line is a unity line (x = y). All points lie above the unity line, indicating that the MUs were higher for all FFF plans. The scatter plot is made in MATLAB.

The number of MUs were significantly greater for each individual arc in the FFF plans, compared to the corresponding arcs of the 6MV plans ($p = 1.7 \cdot 10^{-6}$). Figures 23 and 24 shows scatter plots of the MUs for each arc of the 6MV and FFF plans respectively. The MUs are plotted versus the gamma pass rate of each arc. The MUs for each patient, both total and for individual arcs, can be found in appendix A (table A10). Figure 25 shows the total MUs vs total gamma pass rate for the 6MV and FFF plans. The trend lines plotted indicates that the pass rates for the FFF plans decreases with increasing MUs. This is not the case for the 6MV plans.

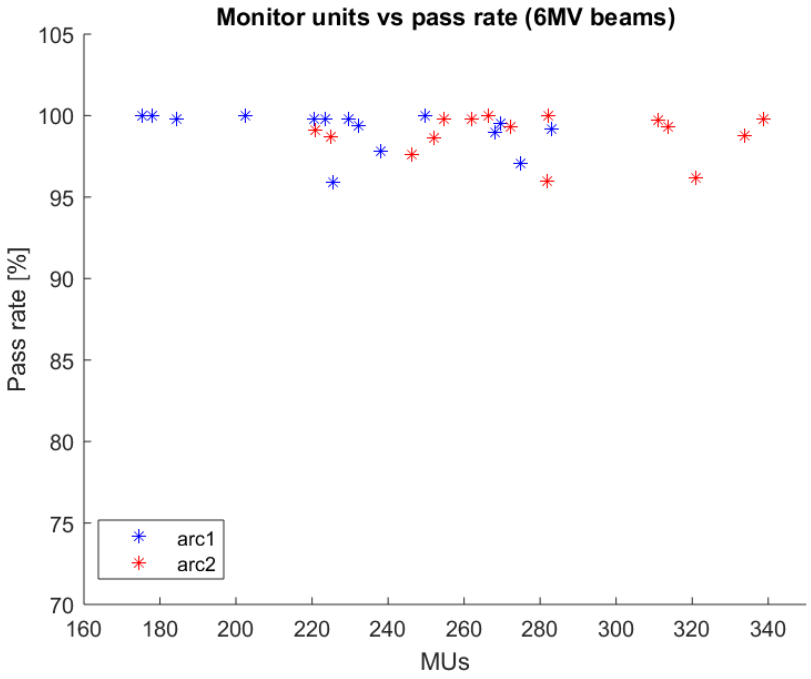

Figure 23: Scatter plot showing the MUs vs pass rates for 6MV plans. The plot is made in MATLAB.

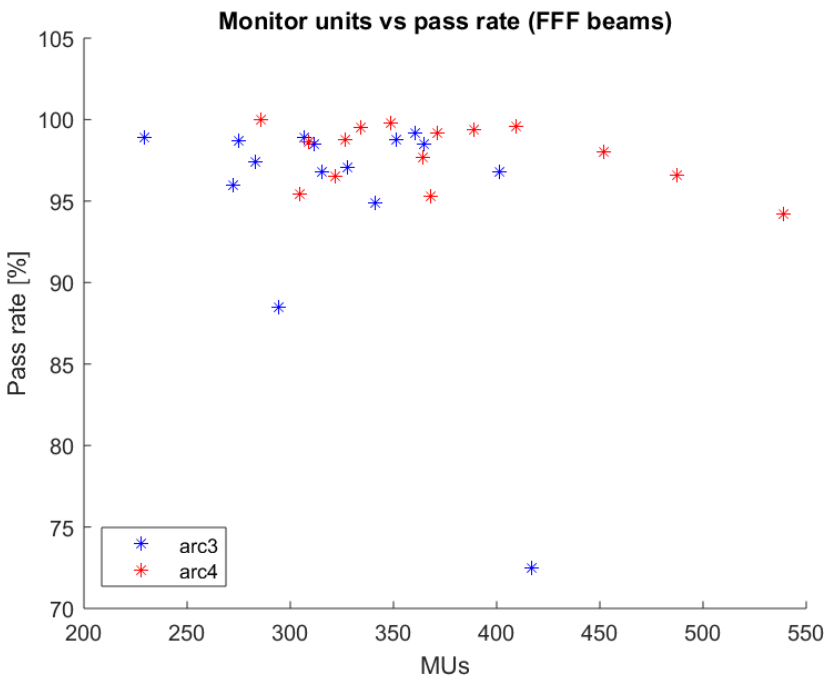

Figure 24: Scatter plot showing the MUs vs pass rates for FFF plans. The plot is made in MATLAB.

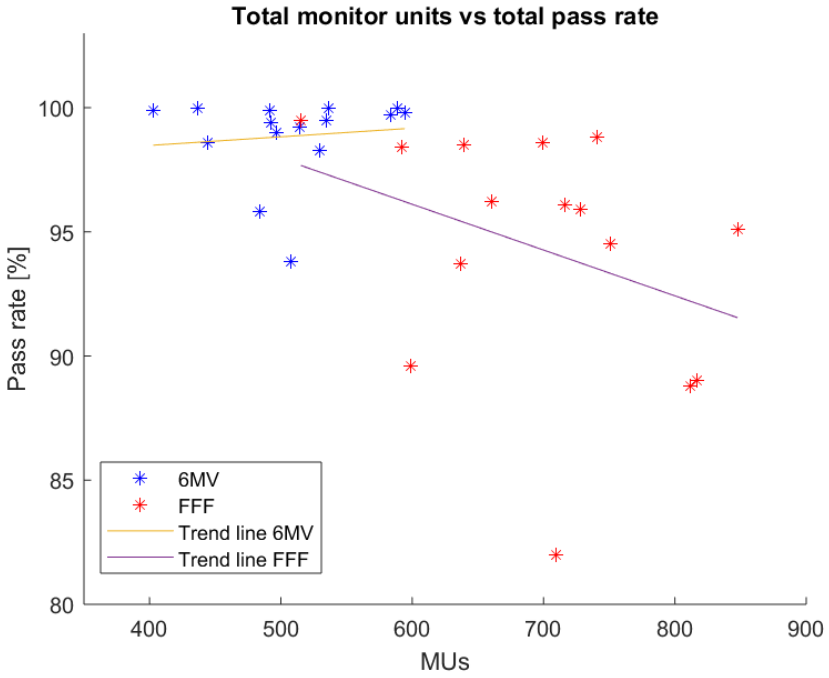

Figure 25: Scatter plot showing the total MUs vs the total gamma pass rate for both 6MV and FFF plans. Trend lines are also included for both 6MV and FFF plans. The plot is made in MATLAB.

4.2.3 Delivery times

Figure 26 shows the measured delivery times for 6MV versus FFF beams, with the individual arcs compared. It can be noticed from this plot that delivery times for the second arc in both 6MV and FFF plans (arc2 and arc4) were higher than the first arc. In addition, the delivery times for 6MV arcs were in general higher than that of the FFF arcs. However, statistical analysis of the delivery times of corresponding arcs for 6MV versus FFF plans returned p = 0.09, meaning that the delivery times of individual corresponding arcs were not significantly different. The total delivery times for the 6MV and FFF plans can be seen in figure 27. The total delivery times for 6MV plans were not significantly different from total delivery times of the FFF plans (p = 0.25). Both measured and RayStation estimated delivery times can be found in appendix A (tables A11 and A12).

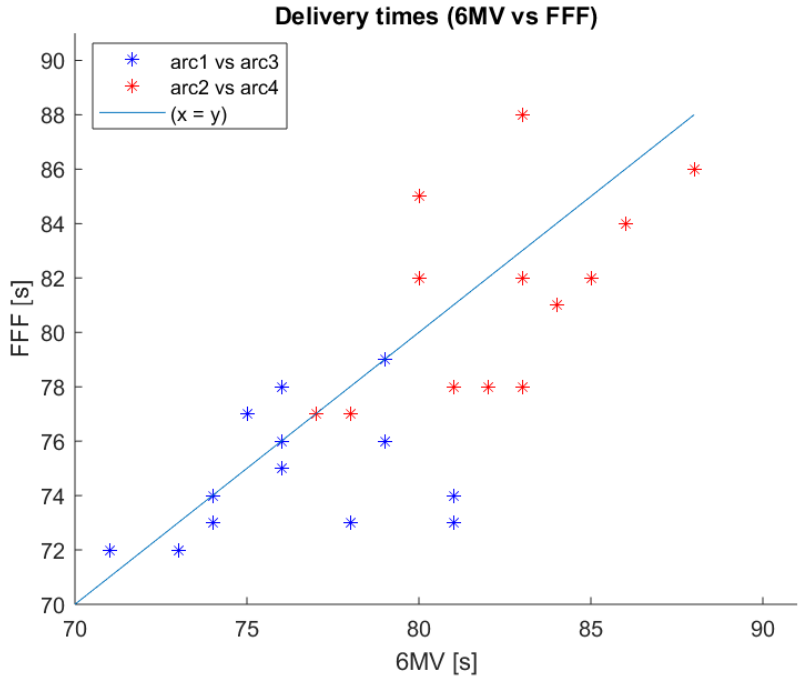

Figure 26: Scatter plot showing measured delivery times for each arc of the 6MV versus FFF plans. The blue line is a unity line (x = y). Points lying below this line indicate longer delivery time for 6MV plans, and vice versa The plot is made in MATLAB.

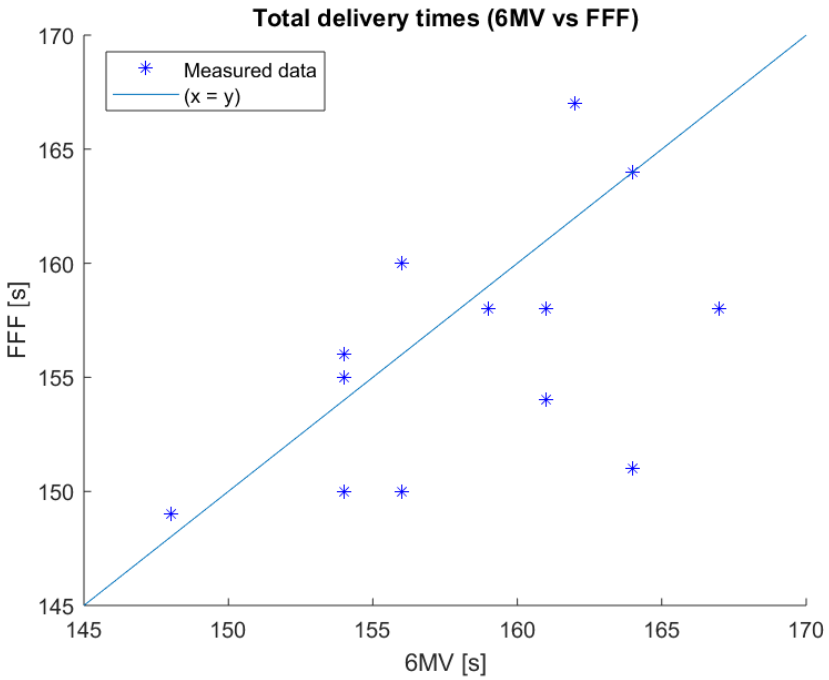

Figure 27: Scatter plot showing total measured delivery times for 6MV versus FFF plans. The blue line is a unity line (x = y). Points lying below this line indicate longer delivery time for 6MV plans, and vice versa. The plot is made in MATLAB.

Figures 28 and 29 shows measured delivery times versus RayStation estimated delivery times for 6MV and FFF plans respectively. Statistical analyses of these data returned $p = 1.7 \cdot 10^{-6}$ and $p = 6.8 \cdot 10^{-4}$ respectively. This implies that the RayStation estimated delivery times were higher than the measured delivery times, both for 6MV and FFF plans.

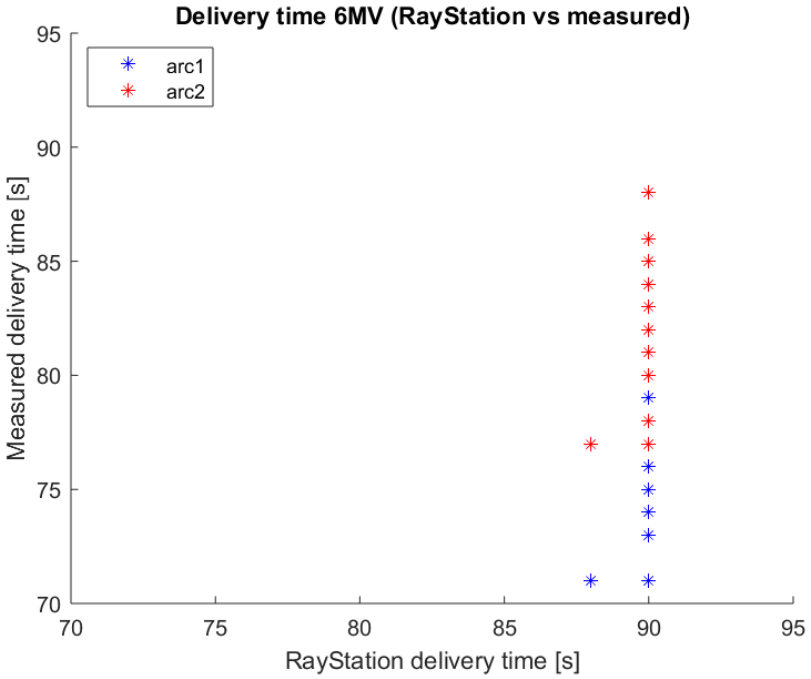

Figure 28: Scatter plot showing RayStation estimated delivery times vs measured delivery times for 6MV plans. The plot is made in MATLAB.

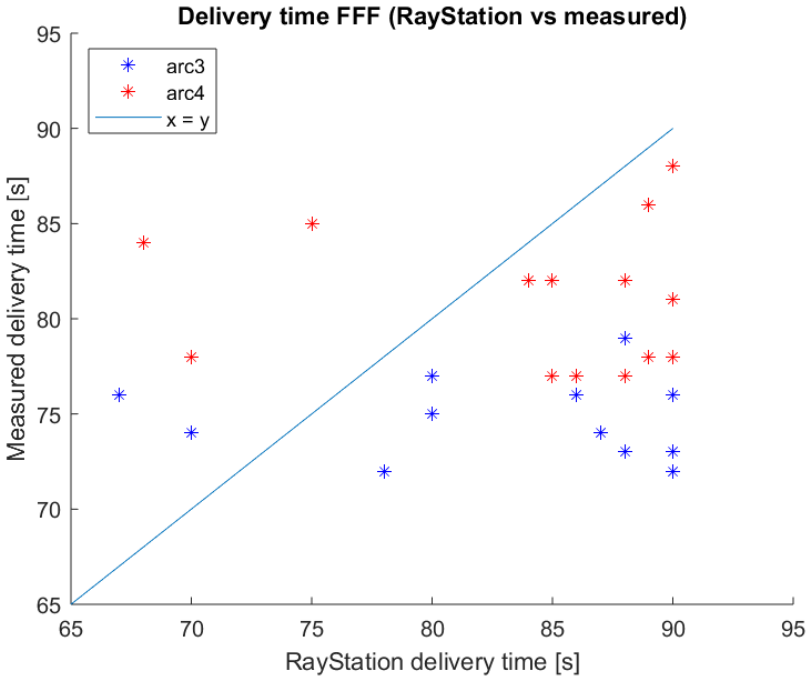

Figure 29: Scatter plot showing RayStation estimated delivery times vs measured delivery times for FFF plans. The blue line is a unity line (x = y). Points lying below this line indicate longer RayStation estimated delivery time, and vice versa. The plot is made in MATLAB.

4.2.4 PTV volumes

Figure 30 shows a scatter plot for the total PTV volumes versus the total gamma pass rate for each patient. Trend lines are included in the plot. It can be noticed that the total pass rates decreases as the total PTV volume increases, both for 6MV and FFF plans.

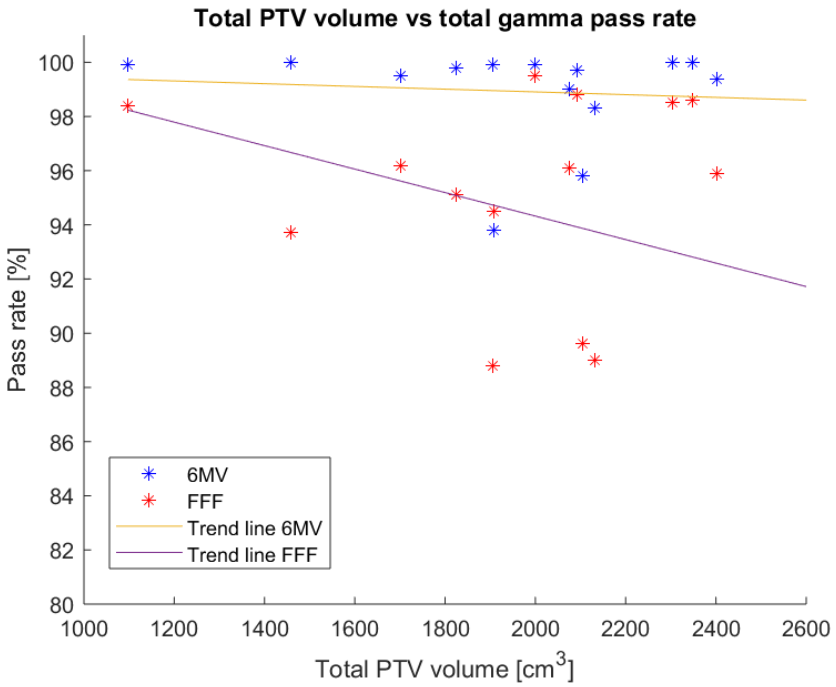

Figure 30: Scatter plot showing the total PTV volume versus the total gamma pass rate for each patient. Trend lines are also included for both 6MV and FFF plans. The plot is made in MATLAB.

The relative PTV boost volume is plotted against pass rate in figure 31, with trend lines included. As the trend lines indicate, the total pass rates for the 6MV and FFF plans slightly increased and decreased respectively, with increasing relative PTV boost volume.

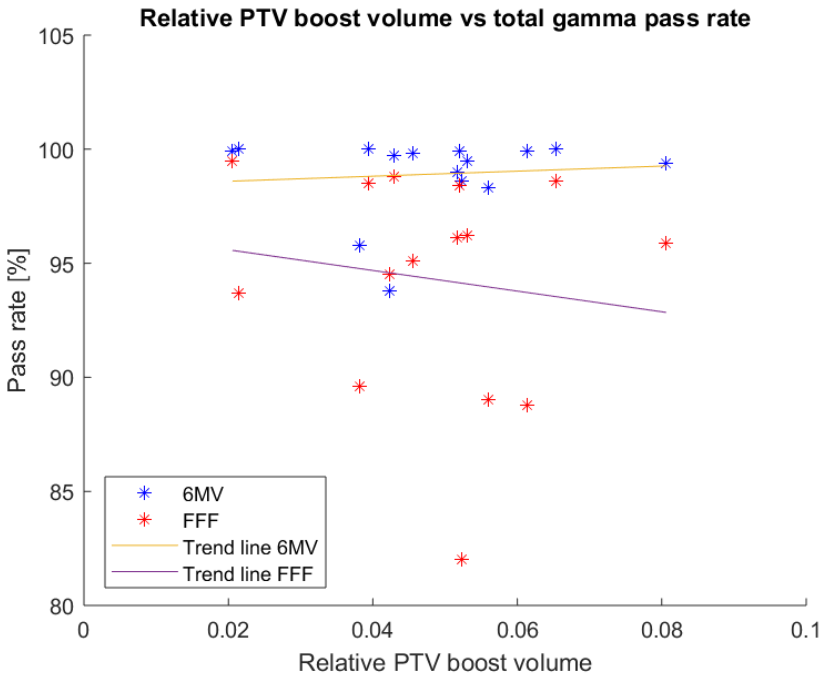

Figure 31: Scatter plot showing the relative PTV boost volume versus the total gamma pass rate for each patient. The relative PTV boost volume is the volume of the PTV-N(#)s divided by the total PTV volume (PTV-T + PTV-E + PTV-N(#)). Trend lines are also included for both 6MV and FFF plans. The plot is made in MATLAB.

5 Discussion

The main priority of the treatment plan optimization was to fulfill the dose constraints for both primary and LN target volumes. This was achieved for all plans, both 6MV and FFF. As seen in figure 15, several OAR and help structure constraints could not be fulfilled, which was the second priority. These constraints were exceeded slightly more frequently in FFF plans than in the standard 6MV plans. In terms of how much the constraints were exceeded, the 6MV and FFF plans were roughly equal. In a study on postoperative VMAT treatment of cervical cancer, Zhang et al found that the target volume dose coverage and OAR sparing was about equal for standard 6MV and 10MV plans compared to FFF plans with the same energies [11]. This is similar to what was found in this study. In terms of OAR sparing, VMAT FFF are then likely more useful for other cancer types, as it has been shown to improve OAR sparing in e.g nasopharyngeal carcinoma [44] and hypopharynx carcinoma [45].

The main dose constraint issue was the "GTV-T+10mm" structure, which exceeded its dose constraint (maximum 46.6 Gy) in all plans. The purpose of this auxiliary structure was to reduce hot spots in OARs in the region around the primary pelvic target, especially in the rectum and the bladder, but also the sigmoideum. When the primary target volume receives an additional dose from BT, these nearby OARs will also be irradiated to some extent, and so the "GTV-T+10mm" structure aimed to keep the EBRT dose in this region below 46.4 Gy. The rectum and the bladder overlapped with the "GTV+10mm" in all but 2 patients, and in some patients the rectum and the bladder overlapped with GTV-T as well. An option would be to specifically optimize the dose distribution in these overlapping regions only. In such cases, auxiliary structures could be made for the overlapping regions, and dose objectives could be defined to reduce the dose in these regions. But, due to differences in bladder and rectum filling, movement of the uterus etc. the anatomy of a patient can alter notably between EBRT treatments. Treatment planning optimization based on such overlapping regions, might then be in vain. Therefore, the strategy of using the "GTV-T+10mm" structure for the above mentioned purpose was chosen, with a maximum dose constraint in a well

defined area around the GTV-T.

The "GTV-T+10mm" structure was enclosed by the PTV-T structure in all patients, and in some patients also by the CTV-T. These structures had prioritized dose constraints that aimed to keep the dose at about 45 Gy in the same area. PTV-N(#)s were generally localized laterally far from the "GTV-T+10mm", but in some cases, these were also localized close to the primary pelvic target volume, and hence close to the "GTV-T+10mm". This is visualized in figure 10. In a few cases, the "GTV-T+10mm" even overlapped with a PTV-N(#), initially. Because of such overlapping with PTV-N(#)s, and enclosure of the "GTV-T+10mm" within PTV-T and CTV-T, the optimization algorithm would have difficulties finding a suitable compromise to satisfy the dose constraints all structures. For this reason, the "GTV-T+10mm" structure was in this study cropped around the PTV-N(#) structures with which it initially overlapped. The purpose of this was to enable a high dose to the PTV-N(#), and at the same time keep the "GTV-T+10mm" dose below 46.4 Gy. However, the latter was not possible in any plans. Attempts to increase the objective weight for the "GTV-T+10mm" structure decreased the target structure doses below their minimum constraints, which was not allowed. A cropping of "GTV-T+10mm" around PTV-N(#)s with an additional margin could be an alternative to the cropping strategy used in this study. This might have contributed to reaching the dose constraint aim for the "GTV-T+10mm", but at the cost of less control of the dose level in the region between the "GTV-T+10mm" and the PTV-N(#)s. Even though the defined "GTV-T+10mm" constraint could not be met in any plans, the objective is considered by the optimization algorithm. Therefore, the aim of reducing the dose in this region will be achieved to some extent. As seen in figure 16, the "GTV-T+10mm" structure exceeded its dose constraints with less than 3 Gy in most cases. As this structure is an auxiliary structure, and not an OAR, such exceedings can be tolerated in a clinical setting. Both the size of this help structure and the maximum dose constraint may be adjusted to get a more robust calculation, and secure that the nearby OARs in this region will not receive too high doses from the EBRT. This is not further considered in this work, but should be considered for future work. It should also be noted that

because of small alterations in anatomy, as discussed above, the RayStation estimated doses is not necessarily exactly equal the actual delivered doses. However, daily CT images are taken for verification, to ensure that this error is as small as possible.

The dose volume constraints for the rectum and bowel were also hard to fulfill in several cases (figure 15). As seen in figure 16 the absolute exceedings measured in Gy were highest for the rectum dose volume constraints. The constraint of maximum 95% at 30 Gy were exceeded with about 7-8 Gy in median, meaning that 95% of the rectum volume received a dose of about 37-38 Gy in median. The 85% rectum volume exceeded its dose volume constraint with half of that of the 95% volume in median. From figure 17, it can be seen that the rectum dose volume constraints were also exceeded the most in absolute percent. In extreme cases 100% of the rectum volume were within the 30 Gy and 40 Gy level. The bladder constraint were exceeded to a somewhat lesser extent. The dose volume constraints for the rectum and the bladder can be difficult to fulfill in many cases, because of the positioning of these organs close to the cervix. In several patients these OARs also overlapped with the PTV-T. But even if the dose volume constraints for the rectum and bladder were exceeded frequently, the maximum dose constraints for these OARs were fulfilled in all patients, which is commonly prioritized over the dose volume constraints. The bowel bag is located more laterally to the cervix. But because of its large volume and varying geometry, the bowel bag might also be exposed to a larger dose than what is desired. In extreme case, over 500 additional cubic centimeters were lying at the 30 Gy dose level (figure 18). However, the dose exceedings to the most irradiated 250cm^3 and 500cm^3 were mostly below 5 Gy. In addition, the maximum dose constraint for the bowel bag was exceeded with less than 3 Gy in all plans but one. The maximum dose constraints were exceeded for the bowel bag, femoral heads and the spinal canal in some cases. Slight exceedings can be tolerated for bowel bag and femoral heads in a clinical setting, but exceeding of the maximum dose constraint for the spinal canal is normally not tolerated. However, because the target dose coverage was the main priority, and that the spinal canal constraints were only exceeded slightly (figure 16), the plans were approved. For all constraints, the absolute dose exceedings were roughly equal for 6MV plans and FFF

plans. No results could be found to conclude otherwise. The dose constraints for the body, kidneys and sigmoid were fulfilled in all plans, both 6MV and FFF. All in all, this is a good representation of the challenges faced by medical physicists and radiation therapists in a clinical setting. The desire of delivering high doses to target volumes while keeping the OAR doses low cannot always be satisfied, and so appropriate priorities must then be made.

The HIs of the 6MV plans were significantly lower than that of the FFF plans ($p = 0.02$), implying a better homogeneity for 6MV plans. However, both 6MV and FFF plans had HIs in the same order of magnitude, and so the clinical relevance may be considered negligible. Both were considered to be satisfactory with respect to homogeneity of the dose distributions. As stated in section 2.3.8, there are other possible definitions of the HI. Pathak and Vashisht [46] did a comparison of 5 HI definitions in relation to IMRT of cervical cancer, among them the S-index proposed by Yoon et. al in 2007 [47]. The HI included in their comparison was defined as $(D_{2\%} - D_{98\%})/D_{pr}$, where $D_{2\%}$ and $D_{98\%}$ are the doses to 2% and 98% of the PTV respectively, and D_{pr} is the prescribed dose. Different definitions of the HI yielded different quantitative measurements of the homogeneity, which illustrates that an exact measure of the homogeneity is not trivial. However, as the purpose of calculating HIs in this study was comparison of 6MV and FFF plans, the choice of definition was not a major issue. A more relevant issue would be comparisons of the found HIs with other studies. Both Zhang et. al [11] and Kumar et. al [35] used the same definition of HI as used in this study, for postoperative FFF VMAT treatment of cervical cancer and FFF rapid arc RT planning for cervical carcinoma, respectively. Zhang et.al found a mean HI of 1.11 for standard 6MV VMAT plans, and 1.12 for FFF VMAT plans. Kumar found respective HIs of 1.05 and 1.06. In both studies the differences between standard 6MV and FFF HIs were found to be significant, even though the differences were small. A similar result was also found in this study, with the mean HIs from this study being somewhere in between the above mentioned HIs. It is therefore considered as a reasonable result.

The PCIs for the 6MV and FFF were calculated as described in section 3.4. The

reason for splitting the PCI calculation into 3 different regions was to examine if the conformity of the 6MV plans were better than that of the FFF plans in these regions, or vice versa. A PCI = 1 implies perfect conformity, and so the results might suggest that the conformity of both 6MV and FFF plans were relatively poor. However, this is not an exact conclusion. Because of the choices of PIVs and TVs in the different regions, the PCIs were likely to be less than 1. In the PTV_45Help region the dose objective was set to be at least 42.75 Gy to 95% of the volume (table 2). A PIV = 45 Gy isodose volume would then not be likely to overlap with the entire TV = PTV_45Help volume. The calculated PCI in this region would then indicate a poor conformity. In the regions with positive LNs, the CTV-N(#)s (55 and 57.5) were defined as the TVs, and the 55 Gy and 57.5 Gy isodose volumes were defined as corresponding PIVs. These isodose volumes will not only be confined to the CTV-N(#)s, but also in parts of the surrounding PTV-N(#)s. Therefore, the PIVs and TVs in these regions would not overlap perfectly. Because of this, the PCIs in these regions would also indicate a sub-optimal conformity. The TVs and PIVs could have been chosen differently in the different regions, to determine the PCIs more exactly. One possibility would be to choose the 42.75 Gy isodose volume as the PIV in the PTV_45Help region. This would give a higher PCI, as these volumes will overlap to a larger extent. Another possibility would be to choose the PTV-N(#)s as TVs, rather than the CTV-N(#)s in the LN regions. But as the dose objectives for the PTV-N(#)55 and PTV-N(#)57.5 were minimum 50 Gy and minimum 52 Gy respectively, corresponding PIVs must had been chosen to appropriately to acquire the real conformity. Other choices for TVs and PIVs could also have been suitable in the different regions. However, the main purpose of calculating the PCIs was to compare the conformity of the 6MV plans with that of the FFF plans. The choice of PIVs and TVs in different regions were therefore satisfactory for this study. The results showed no significant difference in PCIs in any regions, implying that the conformity of the 6MV and FFF plans were equal.

As with the HI, there are many different ways to define the conformity index. Park et al compared 9 different conformity indices [48], and proposed additional two indices for calculating conformity. As different definitions of conformity index has different

advantages and disadvantages, the choice is dependent on the purpose. For comparison of 6MV and FFF plan conformities, the choice of PCI in this study was adequate, as it will be calculated in the similarly for both plans. Even though it was not explicitly expressed in their article that they used the *Paddick* conformity index, the same definition of CI (as PCI) was used by Zhang et al [11]. They found a mean CI of 0.78, for both standard 6MV and FFF plans in their study of postoperative VMAT treatment for cervical cancer. This is a slightly better conformity than what was found in this study. However, the article by Zhang et al. expressed that the PTV was used as TV, and the prescribed isodose to this volume was used as PIV. As these volumes are supposed to overlap perfectly, this choice of TVs and PIVs is likely to yield a good CI. The fact that the CIs for 6MV and FFF plans were not statistically different, is in correspondence with what was found in this study.

The total gamma pass rate was significantly higher for the 6MV plans than for the FFF plans ($p = 1.8 \cdot 10^{-4}$), and every 6MV plan had a gamma pass rate satisfying the clinical criterion of at least 90%. There was only one patient where the total gamma pass rate was higher for the FFF plan than for the 6MV plan. This suggests that the 6MV plans can be delivered more accurately by a clinical linac, than the FFF plans. However, 11 of 15 the FFF plans were satisfying the clinical criterion of at least 90% gamma pass rate. The dosimetric delivery of FFF plans has been shown to be acceptable in other studies as well, both for IMRT, rapid arc and VMAT-stereotactic ablative body radiotherapy [49, 50].

4 of the FFF plans had a gamma pass rate below the 90% criterion. For 3 of these patients, each individual arc had a gamma pass rate of more than 90%. However, because of coinciding errors in each arc, the total gamma pass rates for these plans fell below the passing criterion. The 4 patients were further investigated to examine if there were specific issues with the treatment delivery in specific regions, e.g the LN targets. The recorded data showed no specific regions where neither the absolute or relative dose differences, nor the gamma index, were higher than in other regions. In the gradient area of the beam the relative dose difference can be large, because small

changes in position can lead to large differences in doses. For patient 2, however, it was noticed that the relative dose differences were largest at the center, and not in the gradient region. The largest differences and gamma ratios seemed to be localized randomly over the PTV-T, PTV-E and boost PTVs for all 4 patients. Determination of any specific regions causing poor deliveries could not be done from the measured data. Measurements in RayStation, done after the QA measurements, showed that a few patients had target volumes that stretched over 30 cm in the craniocaudal direction. This was the case for 3 of the 4 patients (patients 2, 7 and 14) in which the FFF plans had a pass rate below 90%. The detector plates of the phantom was 200mm$\times$200mm, and so for long target volumes, one single measurement might not be adequate to yield sufficient data. However, the corresponding 6MV plans, for the 3 mentioned patients, were all delivered with a satisfying gamma pass rate, which could indicate that a possible loss of data due to long target volumes was not necessarily critical. Regardless, in order to improve the assessment and localization of specific issues in the FFF plans, the QA measurements could have been carried out more thoroughly. The Delta4 software offers to split VMAT plans for long targets into two separate plans. Instead of measuring in the region covered by the detector plates of the phantom only, separate measurements can be done for the cranial and the caudal half of the target. This might improve the possibility of pointing out specific regions with large errors, and should be considered for future work. The dose range used in these measurements was 50%-500% of the maximum dose in the QA plan, which is in correspondence with clinical practice. Increasing this dose range could improve the possibility of determining regions with large errors, and should also be considered in future work on this issue.

It has been shown that the MUs required for delivering FFF plans are greater than for standard 6MV plans, e.g in VMAT-stereotactic ablative body radiotherapy [49]. This was also the case in this study. The number of MUs required were significantly greater in FFF plans than 6MV plans, both totally ($p = 6.1 \cdot 10^{-5}$) and for corresponding arcs ($p = 1.7 \cdot 10^{-6}$). This is a consequence of the inhomogeneous nature of the FFF beams leading to more modulated plans (requiring more MUs) than standard 6MV plans. Increased total MUs seemed to decrease the gamma pass rate for the FFF plans, as seen

in figure 25. Because of the high dose rate of the FFF beams, a rapid MLC modulation is required to deliver the prescribed dose correctly. This is not a critical issue in the optimization in the treatment planning system, but when it comes to the actual delivery the rapid MLC modulation required may not be achieved, because of the complex geometries of the target volumes in cervical cancer. As the target volumes increase, and then possibly also the geometrical complexity, these rapid MLC modulations might be even harder to achieve. Rapid MLC modulations are often not required in the cases of certain lung and brain cancers, because the target volumes tend to be smaller and have less complex shapes [51]. In such cases, FFF beam delivery are a feasible tool [33, 52]. FFF beams are also used at St. Olavs Hospital in stereotactic treatments. As seen in figure 25, the total gamma pass rate for 6MV plans seemed to increase slightly with increasing MUs. However, with 15 6MV treatment plans this slight increase is likely observed because of random variations in the 6MV plans. With an increased number of 6MV treatment plans, a possible correlation between increased MUs and increased pass rate could have determined more precisely. This is also true for the FFF plans. However, the 15 FFF plan pass rates decreased with a much steeper gradient, which is unlikely to occur because of random variations only.

Studies have shown that FFF beams can reduce the treatment time [11, 34], which is a main advantage of using FFF beams. In this study, the total measured FFF plan delivery times were mostly shorter than for the corresponding 6MV plans. However, the delivery time differences were only in a matter of seconds, and they did not differ significantly, neither in total delivery times ($p = 0.25$), nor in individual arc delivery times ($p = 0.25$). With an increased number of patient treatment plans, these differences between 6MV and FFF plan delivery times might have been shown to be statistically significant. But even if the differences in delivery times had been shown to be significant, the clinical relevance would likely be negligible. The largest difference observed in delivery times for 6MV and FFF plans was 13 seconds. With total delivery times in the order of about 160 seconds, such a difference does not contribute to saving clinical resources, nor improving patient comfort, to an appreciable extent.

As stated in section 3.3, the actual delivery times were measured manually using a stopwatch. This is a source of error, as it is practically impossible to start and stop the watch at exactly corresponding times for all of the 30 treatment plan deliveries. To make these measurements more precisely, a software including a timer function connected to the linac delivery would be suitable to determine the exact delivery times. However, it is unlikely that the uncertainty in the manual measurements was more than 1 second, and so the end result is practically the same.

RayStation estimated delivery times were significantly higher than measured delivery times, both for 6MV and FFF plans. It should be noticed that the RayStation estimated delivery times for the 6MV plans were 90 seconds in all but one plan (figure 28). This is probably because the plans are made with a time limitation of maximum 90 seconds per arc, and therefore this is also the RayStation estimated delivery time. However, this was a default setting in RayStation, which was not altered in any of the 6MV plans. For the FFF plans, the RayStation estimated times were lower than 90 seconds, even though no alterations were made to change the maximum delivery time limitation for these plans. As seen in figures 28 and 29 there are notable differences between measured and RayStation estimated delivery times for both 6MV and FFF plans. This is not a critical issue, but it is probably due to the fact that when a treatment plan is transferred to a linac, it is the linac that controls the plan delivery in terms of the actual dose rate, MLC modulation and gantry speed. The main priority is that the MLC shape at every control point, and the number of MUs that are delivered between the control points, are correct. Then the actual delivery time is dependent on the aforementioned parameters only, and it is not affected by estimated delivery time.

When evaluating the total PTV volume versus the total gamma pass rates (figure 30), increasing PTV volume seems to decrease the total pass rate for FFF plans. This is a reasonable result, since increased PTV volumes can increase the complexity of the PTV volume geometries. As discussed above, this can cause problems for satisfactory FFF plan delivery. The decrease of total gamma pass rate with increasing PTV volume can also be seen for 6MV plans. However, this is a very slight decrease compared to

that of the FFF plans. In addition, a doubling of the total PTV volume decreased the 6MV pass rate with less than 1%. Such a difference is not an issue in clinical practice, especially since the pass rate is close to 100%. With only 15 samples, this slight decrease can also be due to random variations in the treatment plans. This could also be the fact for the FFF plans, but the decreasing trend is notably greater for than for the 6MV plans, and is considered unlikely to be due to random variations only. When evaluating the relative PTV boost volumes (PTV-N(#)s) versus the total gamma pass rates, the pass rates does not change dramatically. Figure 31 shows that the pass rates for the FFF plans decreases with increasing relative PTV boost volume. However, this a slight decrease. Similary, the 6MV plan pass rates seem to increase slightly with increasing relative PTV boost volume. These changes are not significantly large, and might be caused by random variations in each plan. Such variations can strongly affect the calculated trend line when the number of samples are limited to 15 in each case. A greater number of plans would therefore be required to assess this issue more exactly.

It should be noted that the results are mainly analyzed based on the total plans, but also the individual arcs. However, the corresponding arcs of 6MV and FFF plans (e.g arc1 and arc3) do not necessarily treat the same regions of the target volumes. E.g. arc1 for the 6MV beam might focus on the cranial part of the target volume, while arc3 for the corresponding FFF beam is focused on the caudal part. If there is such a difference, there will naturally be differences in the measured parameters. Therefore, a direct comparison between corresponding arcs does not necessarily reflect the difference in quality of the two plans. Therefore, the total plans have been the main focus.

All in all, both standard 6MV treatment plans and FFF plans could be made satisfying the EMBRACE II protocol dose constraints. There were some difficulties reaching all aims for both target volumes and OARs, but this is also a common issue in a clinical setting. Assessments can be done as to whether some of the constraints should be altered, although this is not considered in this study. OAR constraints were exceeded slightly more frequently in FFF plans than in standard 6MV plans. The homogeneity

were also significantly better for 6MV plans than for FFF plans, even though this difference was small. The clinical relevance of this finding may therefore be slight. The conformity of the 6MV and FFF plans were statistically similar. Even if both 6MV and FFF plans were roughly equal in terms of treatment planning aims, the 6MV plans were more precisely delivered by a clinical linac. The 6MV plans were significantly better than the corresponding FFF plans with respect to gamma pass rates. The FFF plan pass rates were also decreasing with increasing MUs and increasing PTV volume, notably more than 6MV plans. The measured delivery times for the 6MV and FFF plans were also similar. This was expected to be significantly lower for FFF plans, as this is one of the main advantages of FFF beams.

In cervical cancer patients with lymph node metastases, the target volumes are often complex and inhomogeneous. Even though the standard 6MV and FFF treatment plans were about equal with respect to dose distribution in the treatment planning system, the 6MV plans were more accurately delivered by a clinical linac. The standard 6MV VMAT SIB plans are therefore preferred to FFF plans, for this patient group.

6 Conclusion

EBRT plans with VMAT and SIB for treatment of cervical cancer with lymph node metastasis were made clinically satisfactory for both standard 6MV and FFF radiation, with about equal target dose coverage, OAR sparing and conformity. The homogeneity were significantly better for 6MV plans than that for the FFF plans, even though this difference was small. The QA measurements showed that 6MV plans were more accurately delivered by a clinical linac, than the corresponding FFF plans. The 6MV plans were found to be significantly better in terms of gamma pass rates. The delivery times for the FFF plans were only marginally reduced compared to the 6MV plans, and no significant difference could be found. For patients with cervical cancer with lymph node metastases, the standard 6MV VMAT SIB plans are therefore preferred to FFF plans.

References

[1] World Health Organization. World Cancer Report 2014. *International agency for research on cancer. IARC Press, Lyon, 2014.*

[2] LA Torre et al. Global cancer statistics, 2012. *CA: A cancer journal for clinicians*, 65(2):87–108, 2015.

[3] G. Engholm et al. Association of the Nordic Cancer Registries; Danish Cancer Society. NORDCAN: Cancer Incidence, Mortality, Prevalence and Survival in the Nordic Countries. Version 7.3 (08.07.2016). `http://www.ancr.nu`. Accessed: 03.04.2018.

[4] Tanderup, K et al. Effect of tumor dose, volume and overall treatment time on local control after radiochemotherapy including MRI guided brachytherapy of locally advanced cervical cancer. *Radiotherapy and oncology*, 120(3):441–46, 2016.

[5] Kidd, E.A et al. Lymph node staging by positron emission tomography in cervical cancer: relationship to prognosis. *Journal of clinical oncology*, 28(12):2108–13, 2010.

[6] Wakatsuki, M et al. Impact of boost irradiation on pelvic lymph node control in patients with cervical cancer. *Journal of radiation research*, 55(1):139–45, 2014.

[7] Feng, CH et al. Simultaneously integrated boost (SIB) spares OAR and reduces treatment time in locally advanced cervical cancer. *Journal of Applied Clinical Medical Physics*, 17(5):76–89, 2016.

[8] Lubgan, D et al. Effective local control of vertebral metastases by simultaneous integrated boost radiotherapy: preliminary results. *Strahlentherapie und onkologie*, 191(3):264–71, 2015.

[9] Fiorentino, A et al. Intensity modulated radiation therapy with simultaneous integrated boost in early breast cancer irradiation. Report of feasibility and preliminary toxicity. *Cancer radiotherapie*, 19(5):289–94, 2015.

[10] Thomas, E et al. Effects of flattening filter-free and volumetric modulated arc therapy delivery on treatment efficiency. *Journal of Applied Clinical Medical Physics*, 14(6), 2013.

[11] Zhang, F et al. A dosimetric evaluation of flattening filter-free volumetric modulated arc therapy for postoperative treatment of cervical cancer. *Oncology and translational medicine.*, 2(4):179–84, 2016.

[12] R Kurman. *Blaustein's Pathology of the Female Genital Tract*. Springer, New York, USA, 4th. ed, 1994.

[13] Obgyn Key. Diseases of the Cervix. `https://obgynkey.com/diseases-of-the-cervix/`. Accessed: 22.03.2018.

[14] Mark Schiffman et al. Human Papillomavirus Testing in the Prevention of Cervical Cancer. *Journal of the National Cancer Institute*, 103(5):368–83, 2011.

[15] Peter JF Snijders et al. HPV-mediated cervical carcinogenesis: concepts and clinical implications. *The Journal of Pathology*, 208(2):152–164, 2006.

[16] M. Nuñoz et al. Against which human papillomavirus types shall we vaccinate and screen? The international perspective. *International journal of cancer*, 111(2):278–85, 2004.

[17] M Schwab. *(2011) Lymphatic System.* Springer, Berlin, Heidelberg, 1994.

[18] Richard S. Snell. *Clinical anatomy for medical students (4th edition).* Little, Brown and Company, Boston/Toronto/London., 1992.

[19] G.J. Romanes. *Cunningham's textbook of anatomy (11th edition).* Oxford university press, Ely House, London W., 1972.

[20] S. Pecorelli. Revised FIGO for carcinoma of the vulva, cervix, and endometrium. *International Journal of Gynecology and Obstetrics*, 105(2):103–4, 2009.

[21] Helsedirektoratet. *Nasjonalt handlingsprogram med retningslinjer for gynekologisk kreft.*, 2016. Accessed: 21.04.2018.

[22] Cancer Registry of Norway. *Cancer in Norway 2016 - Cancer incidence, mortality, survival and prevalence in Norway*, Cancer Registry of Norway, Oslo, 2016.

[23] GYN GEC-ESTRO. *EMBRACE: A european study on MRIguided brachytherapy in locally advanced cervical cancer (study protocol)*, 2008. Accessed: 23.03.2018.

[24] Haie-Meder, C et al. Recommendations from Gynaecological (GYN) GEC-ESTRO Working Group (I): concepts and terms in 3D image based 3D treatment planning in cervix cancer brachytherapy with emphasis on MRI assessment of GTV and CTV. *Radiotherapy and Oncology: journal of the European society for therapeutic radiology and oncology*, 74(3):235–245, 2005.

[25] Sturdza, A et al. Image guided brachytherapy in locally advanced cervical cancer: Improved pelvic control and survival in RetroEMBRACE, a multicenter cohort study. *Radiotherapy and oncology*, 120(3):428–433, 2016.

[26] Mazeron, R et al. Dose-volume effect relationships for late rectal morbidity in patients treated with chemoradiation and MRI-guided adaptive brachytherapy for locally advanced cervical cancer: Results from the prospective multicenter EMBRACE study. *Radiotherapy and oncology*, 120(3):412–19, 2016.

[27] Kirchheiner, K et al. Dose-effect relationship and risk factors for vaginal stenosis after definitive radio(chemo)therapy with image-guided brachytherapy for locally advanced cervical cancer in the EMBRACE study. *Radiotherapy and oncology*, 118(1):160–6, 2016.

[28] GYN GEC-ESTRO. *EMBRACE II: Image guided intensity modulated external beam radiochemotherapy and MRI based adaptive brachytherapy in locally advanced cervical cancer (study protocol)*, 2015. Accessed: 27.01.2018.

[29] Mohamed, SM et al. Assessment of radiation doses to the para-aortic, pelvic, and inguinal lymph nodes delivered by image-guided adaptive brachytherapy in locally advanced cervical cancer. *Brachytherapy*, 14(1):56–61, 2015.

[30] D. Greene and P.C. Williams. *Linear accelerators for radiation therapy (2nd edition)*. Institute of Physics Publishing, Bristol and Philadelphia., 1997.

[31] Mayles Nahum Rosenwald. *Handbook of radiotherapy physics.* Taylor and Francis, 2007.

[32] `https://www.thegreenjournal.com/article/S0167-8140(13)00476-3/fulltext`. Accessed: 02.05.2018.

[33] Aoki, S et al. Flattening filter-free technique in volumetric modulated arc therapy for lung stereotactic body radiotherapy: A clinical comparison with the flattening filter technique. *Oncology letters.*, 15(3):3928–3936, 2018.

[34] Geng, J et al. Stereotactic Radiotherapy for Non-small Cell Lung Cancer with Small Lesions Applying A Flattening Filter Free Clinac. *Chinese journal of lung cancer*, 18(5):301–307, 2015.

[35] Kumar, L et al. Dosimetric influence of filtered and flattening filter free photon beam on rapid arc (RA) radiotherapy planning in case of cervix carcinoma. *Reports of practical oncology and radiotherapy.*, 22:10–18, 2017.

[36] The International Commission on Radiation Units and Measurements. ICRU Report 83: Prescribing, recording, and reporting intensity-modulated photon-beam therapy (IMRT). *(Oxford University Press, Oxford, 2010).*

[37] RaySearch Laboratories AB, Stockholm, Sweden. VMAT optimization in RayStation. `https://www.raysearchlabs.com/globalassets/about-overview/media-center/wp-re-ev-n-pdfs/white-papers/white-paper-3---vmat-aug-2015.pdf`. Accessed: 01.05.2018.

[38] International atomic energy agency. *Technical reports series no. 398. Absorbed Dose Determination in External Beam Radiotherapy. An International Code of Practice for Dosimetry Based on Standards of Absorbed Dose to Water*, 2000. Accessed: 04.05.2018.

[39] Jen-Yu Cheng et al. Simultaneous integrated boost (SIB) of the parametrium and cervix in radiotherapy for uterine cervical carcinoma: a dosimetric study using a new alternative approach. *Br J Radiol*, 89(1068), 2016.

[40] Boyle, J et al. Methods, safety, and early clinical outcomes of dose escalation using simultaneous integrated and sequential boosts in patients with locally advanced gynecologic malignancies. *Journal of Applied Clinical Medical Physics*, 135(2):239–43, 2014.

[41] Eric J. Hall and Amato J. Giaccia. *Radiobiology for the radiologist*. Lippincott Williams and Wilkins, Philadelphia, USA, 7th. ed, 2012.

[42] I. Paddick. A simple scoring ratio to index the conformity of radiosurgical treatment plans. *Journal of neurosurgery*, Dec 93(supp3):219–22, 2000.

[43] Low, DA et al. A technique for the quantitative evaluation of dose distributions.. *Medical physics*, 25(5):656–61, 1998.

[44] Zhuang, M et al. Reirradiation of nasopharyngeal carcinoma focusing on volumetric modulated arcs with flattening filter-free beams. *The British journal of radiology*, 88(1052), 2015.

[45] Dobler, B et al. Simultaneous integrated boost therapy of carcinoma of the hypopharynx/larynx with and without flattening filter - a treatment planning and dosimetry study. *Radiation oncology*, 12(1):114, 2017.

[46] Pathak, P. and Vashisht, S. A quantitative analysis of intensity-modulated radiation therapy plans and comparison of homogeneity indices for the treatment of gynecological cancers. *Journal of medical physics*, 38(2):67–73, 2013.

[47] Yoon, M et al. A new homogeneity index based on statistical analysis of the dose-volume histogram. *Journal of applied clinical medical physics*, 8(2):9–17, 2007.

[48] Park, J.M et al. New conformity indices based on the calculation of distances between the target volume and the volume of reference isodose. *The British journal of radiology*, 87(1043), 2014.

[49] Chung, JB et al. Comparison of VMAT-SABR treatment plans with flattening filter (FF) and flattening filter-free (FFF) beam for localized prostate cancer. *Journal of applied clinical medical physics*, 16(6):302–313, 2015.

[50] Lang, S et al. Pretreatment quality assurance of flattening filter free beams on 224 patients for intensity modulated plans: a multicentric study. *Medical physics*, 39(3):1351–6, 2012.

[51] Stieler, F et al. Intensity modulated radiosurgery of brain metastases with flattening filter-free beams. *Radiotherapy and oncology*, 109(3):448–51, 2013.

[52] Fiorentino, A et al. Stereotactic ablative radiation therapy for brain metastases with volumetric modulated arc therapy and flattening filter free delivery: feasibility and early clinical results. *La Radiologia medica*, 122(9):676–682, 2017.

Appendices

A Tables

Table A1: The HIs for the 6MV and FFF plans.

Patient (#)	6MV	FFF
1	1.074	1.087
2	1.062	1.084
3	1.056	1.054
4	1.101	1.100
5	1.075	1.077
6	1.063	1.062
7	1.073	1.079
8	1.073	1.082
9	1.066	1.069
10	1.072	1.075
11	1.067	1.064
12	1.068	1.076
13	1.059	1.057
14	1.094	1.108
15	1.066	1.068

Table A2: The PCIs for the 6MV and FFF plans. PCI_{45}, PCI_{55} and $PCI_{57.5}$ indicate the regions where the PCI are calculated, as described in section 3.4.

	6MV			FFF		
Patient (#)	PCI_{45}	PCI_{55}	$PCI_{57.5}$	PCI_{45}	PCI_{55}	$PCI_{57.5}$
1	0.701	0.551	-	0.667	0.545	-
2	0.698	0.546	-	0.526	0.309	-
3	0.771	0.693	-	0.788	0.635	-
4	0.743	0.492	0.794	0.756	0.504	0.744
5	0.714	0.564	-	0.741	0.593	-
6	0.754	0.444	-	0.712	0.470	-
7	0.744	0.489	0.796	0.724	0.485	0.745
8	0.666	0.553	0.462	0.648	0.535	0.437
9	0.664	0.576	-	0.698	0.562	-
10	0.680	0.493	-	0.671	0.517	-
11	0.670	0.502	-	0.701	0.461	-
12	0.705	0.513	-	0.644	0.497	-
13	0.697	0.502	-	0.737	0.564	-
14	0.702	0.560	0.819	0.663	0.566	0.731
15	0.618	0.457	-	0.660	0.497	-

Table A3: The OAR and auxiliary structures exceeding their dose constraints for patients 1-5 in 6MV plans. The level indicates the result after treatment plan optimization.

Patient (#)	Structure	Constraint	Level
1	GTV-T+10mm	Max 46.4 Gy	51.37 Gy
	Rectum	Max 85% volume at 40 Gy	93.81% (43.47 Gy at 85% volume)
		Max 95% volume at 30 Gy	99.31% (38.53 Gy at 95% volume)
2	GTV-T+10mm	Max 46.4 Gy	51.37 Gy
	Bowel bag	Max 250cm^3 at 40 Gy	417.1cm^3 (44.29 Gy at 250cm^3)
		Max 500cm^3 at 30 Gy	825.3cm^3 (37.45 Gy at 500cm^3)
	Femoral head (left)	Max 50 Gy	50.83 Gy
3	GTV-T+10mm	Max 46.4 Gy	47.2 Gy
	Rectum	Max 85% volume at 40 Gy	90.77% (43.2 Gy at 85% volume)
		Max 95% volume at 30 Gy	99.40% (36.3 Gy at 95% volume)
	Bowel bag	Max 250cm^3 at 40 Gy	314.7cm^3 (43.5 Gy at 250cm^3)
4	GTV-T+10mm	Max 46.4 Gy	47.42 Gy
	Rectum	Max 85% volume at 40 Gy	94.96% (44.39 Gy at 85% volume)
		Max 95% volume at 30 Gy	96.08% (38.13 Gy at 95% volume)
	Bowel bag	Max 250cm^3 at 40 Gy	376.6cm^3 (44.25 Gy at 250cm^3)
		Max 500cm^3 at 30 Gy	704.0cm^3 (35.24 Gy at 500cm^3)
		Max 57.5 Gy	58.08 Gy
	Bladder	Max 75% volume at 40 Gy	76.90% (41.73 Gy at 75% volume)
		Max 85% volume at 30 Gy	85.18% (30.30 Gy at 85% volume)
	Spinal canal	Max 48 Gy	49.00 Gy
5	GTV-T+10mm	Max 46.4 Gy	48.08 Gy
	Rectum	Max 85% volume at 40 Gy	86.90% (41.11 Gy at 85% volume)
		Max 95% volume at 30 Gy	96.20% (31.82 Gy at 95% volume)
	Bowel bag	Max 57.5 Gy	58.43 Gy

Table A4: The OAR and auxiliary structures exceeding their dose constraints for patients 6-10 in 6MV plans. The level indicates the result after treatment plan optimization.

Patient (#)	Structure	Constraint	Level
6	GTV-T+10mm	Max 46.4 Gy	52.99 Gy
7	GTV-T+10mm	Max 46.4 Gy	47.36 Gy
	Rectum	Max 85% volume at 40 Gy	100% (44.29 Gy at 85% volume)
		Max 95% volume at 30 Gy	100% (43.17 Gy at 95% volume)
	Bowel bag	Max 250cm^3 at 40 Gy	288.8cm^3 (41.54 Gy at 250cm^3)
		Max 500cm^3 at 30 Gy	546.4cm^3 (31.61 Gy at 500cm^3)
8	GTV-T+10mm	Max 46.4 Gy	49.94 Gy
	Rectum	Max 85% volume at 40 Gy	87.50% (41.40 Gy at 85% volume)
		Max 95% volume at 30 Gy	100% (36.64 Gy at 95% volume)
	Bowel bag	Max 57.5 Gy	59.88 Gy
	Spinal canal	Max 48 Gy	49.09 Gy
9	GTV-T+10mm	Max 46.4 Gy	47.61 Gy
	Rectum	Max 85% volume at 40 Gy	85.85% (40.53 Gy at 85% volume)
		Max 95% volume at 30 Gy	100% (31.55 Gy at 95% volume)
10	GTV-T+10mm	Max 46.4 Gy	47.09 Gy
	Bowel bag	Max 250cm^3 at 40 Gy	500.7cm^3 (45.19 Gy at 250cm^3)
		Max 500cm^3 at 30 Gy	813.9^3 (40.02 Gy at 500cm^3)
	Femoral head (left)	Max 50 Gy	51.25 Gy
	Femoral head (right)	Max 50 Gy	51.42 Gy

Table A5: The OAR and auxiliary structures exceeding their dose constraints for patients 11-15 in 6MV plans. The level indicates the result after treatment plan optimization.

Patient (#)	Structure	Constraint	Level
11	GTV-T+10mm	Max 46.4 Gy	52.30 Gy
	Rectum	Max 85% volume at 40 Gy	91.42% (43.32 Gy at 85% volume)
		Max 95% volume at 30 Gy	98.40% (35.69 Gy at 95% volume)
	Femoral head (left)	Max 50 Gy	50.19 Gy
12	GTV-T+10mm	Max 46.4 Gy	54.15 Gy
	Rectum	Max 85% volume at 40 Gy	95.03% (43.48 Gy at 85% volume)
		Max 95% volume at 30 Gy	100% (40.01 Gy at 95% volume)
13	GTV-T+10mm	Max 46.4 Gy	48.08 Gy
	Rectum	Max 85% volume at 40 Gy	97.38% (44.08 Gy at 85% volume)
		Max 95% volume at 30 Gy	98.66% (41.88 Gy at 95% volume)
	Bowel bag	Max 250cm^3 at 40 Gy	365.7cm^3 (44.88 Gy at 250cm^3)
		Max 500cm^3 at 30 Gy	500.2cm^3 (30.01 Gy at 500cm^3)
		Max 57.5 Gy	58.78 Gy
14	GTV-T+10mm	Max 46.4 Gy	48.22 Gy
	Bowel bag	Max 250cm^3 at 40 Gy	378.5cm^3 (43.97 Gy at 250cm^3)
		Max 500cm^3 at 30 Gy	706.5cm^3 (35.59 Gy at 500cm^3)
		Max 57.5 Gy	58.97 Gy
15	GTV-T+10mm	Max 46.4 Gy	47.97 Gy
	Rectum	Max 85% volume at 40 Gy	94.40% (43.04 Gy at 85% volume)
		Max 95% volume at 30 Gy	100% (39.20 Gy at 95% volume)
	Bowel bag	Max 250cm^3 at 40 Gy	265.0cm^3 (41.14 Gy at 250cm^3)
		Max 57.5 Gy	57.68 Gy
	Bladder	Max 75% volume at 40 Gy	79.58% (42.14 Gy at 75% volume)
		Max 85% volume at 30 Gy	93.62% (36.45 Gy at 85% volume)
	Femoral head (left)	Max 50 Gy	51.64 Gy
	Femoral head (right)	Max 50 Gy	50.85 Gy

Table A6: The OAR and auxiliary structures exceeding their dose constraints for patients 1-5 in FFF plans. The level indicates the result after treatment plan optimization.

Patient (#)	Structure	Constraint	Level
1	GTV-T+10mm	Max 46.4 Gy	51.08 Gy
	Rectum	Max 85% volume at 40 Gy	93.51% (43.80 Gy at 85% volume)
		Max 95% volume at 30 Gy	100% (38.61 Gy at 95% volume)
	Bowel bag	Max 250cm^3 at 40 Gy	307.0cm^3 (42.24 Gy at 250cm^3)
		Max 500cm^3 at 30 Gy	615.9cm^3 (33.03 Gy at 500cm^3)
2	GTV-T+10mm	Max 46.4 Gy	51.37 Gy
	Rectum	Max 95% volume at 30 Gy	96.52% (31.19 Gy at 95% volume)
	Bowel bag	Max 250cm^3 at 40 Gy	637.8cm^3 (46.59 Gy at 250cm^3)
		Max 500cm^3 at 30 Gy	1079.2cm^3 (43.29 Gy at 500cm^3)
		Max 57.5 Gy	64.21 Gy
	Femoral head (left)	Max 50 Gy	50.23 Gy
	Femoral head (right)	Max 50 Gy	50.73 Gy
3	GTV-T+10mm	Max 46.4 Gy	47.26 Gy
	Rectum	Max 85% volume at 40 Gy	94.09% (44.26 Gy at 85% volume)
		Max 95% volume at 30 Gy	100% (39.03 Gy at 95% volume)
	Bowel bag	Max 250cm^3 at 40 Gy	331.8cm^3 (43.95 Gy at 250cm^3)
		Max 500cm^3 at 30 Gy	502.5cm^3 (30.13 Gy at 500cm^3)
4	GTV-T+10mm	Max 46.4 Gy	47.02 Gy
	Rectum	Max 85% volume at 40 Gy	94.96% (44.52 Gy at 85% volume)
		Max 95% volume at 30 Gy	96.11% (38.15 Gy at 95% volume)
	Bowel bag	Max 250cm^3 at 40 Gy	385.5cm^3 (44.42 Gy at 250cm^3)
		Max 500cm^3 at 30 Gy	692.3cm^3 (35.13 Gy at 500cm^3)
		Max 57.5 Gy	58.09 Gy
	Bladder	Max 75% volume at 40 Gy	76.86% (41.66 Gy at 75% volume)
		Max 85% volume at 30 Gy	85.04% (30.07 Gy at 85% volume)
5	GTV-T+10mm	Max 46.4 Gy	47.84 Gy
	Rectum	Max 85% volume at 40 Gy	86.45% (40.69 Gy at 85% volume)
		Max 95% volume at 30 Gy	96.11% (31.48 Gy at 95% volume)
	Bowel bag	Max 57.5 Gy	58.31 Gy

Table A7: The OAR and auxiliary structures exceeding their dose constraints for patients 6-10 in FFF plans. The level indicates the result after treatment plan optimization.

Patient (#)	Structure	Constraint	Level
6	GTV-T+10mm	Max 46.4 Gy	52.99 Gy
7	GTV-T+10mm	Max 46.4 Gy	47.18 Gy
	Rectum	Max 85% volume at 40 Gy	100% (44.50 Gy at 85% volume)
		Max 95% volume at 30 Gy	100% (43.59 Gy at 95% volume)
	Bowel bag	Max 250cm^3 at 40 Gy	299.7cm^3 (41.87 Gy at 250cm^3)
		Max 500cm^3 at 30 Gy	542.6cm^3 (31.65 Gy at 500cm^3)
8	GTV-T+10mm	Max 46.4 Gy	50.04 Gy
	Rectum	Max 85% volume at 40 Gy	100% (44.27 Gy at 85% volume)
		Max 95% volume at 30 Gy	100% (43.46 Gy at 95% volume)
	Bowel bag	Max 500cm^3 at 30 Gy	512.8cm^3 (30.31 Gy at 500cm^3)
		Max 57.5 Gy	59.51 Gy
	Spinal canal	Max 48 Gy	48.33 Gy
9	GTV-T+10mm	Max 46.4 Gy	47.93 Gy
	Rectum	Max 85% volume at 40 Gy	85.12% (40.07 Gy at 85% volume)
		Max 95% volume at 30 Gy	96.31% (31.61 Gy at 95% volume)
10	GTV-T+10mm	Max 46.4 Gy	47.13 Gy
	Bowel bag	Max 250cm^3 at 40 Gy	495.9cm^3 (45.12 Gy at 250cm^3)
		Max 500cm^3 at 30 Gy	789.4^3 (39.86 Gy at 500cm^3)
	Femoral head (left)	Max 50 Gy	50.05 Gy
	Femoral head (right)	Max 50 Gy	51.52 Gy
	Spinal canal	Max 48 Gy	48.23 Gy

Table A8: The OAR and auxiliary structures exceeding their dose constraints for patients 11-15 in FFF plans. The level indicates the result after treatment plan optimization.

Patient (#)	Structure	Constraint	Level
11	GTV-T+10mm	Max 46.4 Gy	52.72 Gy
	Rectum	Max 85% volume at 40 Gy	91.08% (43.30 Gy at 85% volume)
		Max 95% volume at 30 Gy	98.43% (35.75 Gy at 95% volume)
	Femoral head (left)	Max 50 Gy	50.60 Gy
12	GTV-T+10mm	Max 46.4 Gy	54.44 Gy
	Rectum	Max 85% volume at 40 Gy	99.88% (44.30 Gy at 85% volume)
		Max 95% volume at 30 Gy	100% (42.16 Gy at 95% volume)
13	GTV-T+10mm	Max 46.4 Gy	47.10 Gy
	Rectum	Max 85% volume at 40 Gy	98.14% (44.80 Gy at 85% volume)
		Max 95% volume at 30 Gy	99.07% (44.28 Gy at 95% volume)
	Bowel bag	Max 250cm^3 at 40 Gy	357.7cm^3 (44.58 Gy at 250cm^3)
		Max 500cm^3 at 30 Gy	509.1cm^3 (30.54 Gy at 500cm^3)
		Max 57.5 Gy	58.28 Gy
14	GTV-T+10mm	Max 46.4 Gy	48.08 Gy
	Rectum	Max 85% volume at 40 Gy	85.89% (40.48 Gy at 85% volume)
	Bowel bag	Max 250cm^3 at 40 Gy	455.0cm^3 (44.36 Gy at 250cm^3)
		Max 500cm^3 at 30 Gy	750.4cm^3 (38.85 Gy at 500cm^3)
		Max 57.5 Gy	59.47 Gy
15	GTV-T+10mm	Max 46.4 Gy	48.59 Gy
	Rectum	Max 85% volume at 40 Gy	92.98% (43.29 Gy at 85% volume)
		Max 95% volume at 30 Gy	100% (38.50 Gy at 95% volume)
	Bowel bag	Max 250cm^3 at 40 Gy	255.6cm^3 (40.30 Gy at 250cm^3)
		Max 57.5 Gy	57.96 Gy
	Bladder	Max 75% volume at 40 Gy	79.16% (41.76 Gy at 75% volume)
		Max 85% volume at 30 Gy	94.81% (36.46 Gy at 85% volume)
	Femoral head (left)	Max 50 Gy	51.89 Gy
	Spinal canal	Max 48 Gy	49.02 Gy

Table A9: The gamma pass rates for each individual patient.

	6MV			FFF		
Patient (#)	arc1 [%]	arc2 [%]	Total [%]	arc3 [%]	arc4 [%]	Total [%]
1	97.1	99.8	98.3	98.5	98.0	89.0
2	99.4	100.4	99.9	96.0	94.2	88.8
3	100.0	98.7	99.9	98.9	100.0	99.5
4	99.8	99.3	99.4	96.8	98.8	95.9
5	100.0	98.8	100.0	98.7	97.7	98.5
6	99.8	98.6	100.0	96.8	96.5	93.7
7	99.8	99.1	98.6	94.9	95.3	82.0
8	100.0	96.2	99.0	98.9	99.6	96.1
9	99.5	99.3	99.7	98.8	99.4	98.8
10	99.2	99.7	99.8	99.2	96.6	95.1
11	100.0	99.8	100.0	97.1	99.2	98.6
12	95.9	96.0	93.8	72.5	99.5	94.5
13	99.8	99.8	99.9	97.4	98.6	98.4
14	97.8	97.6	95.8	88.5	95.4	89.6
15	99.0	100.0	99.5	98.5	99.8	96.2

Table A10: MUs for each individual patient. MUs for both arcs are included, as well as the total number of MUs.

	6MV			FFF		
Patient (#)	arc1	arc2	Total	arc3	arc4	Total
1	274.7	254.7	529.4	364.8	452.0	816.8
2	232.3	282.3	514.6	272.4	539.2	811.6
3	178.0	224.8	402.8	229.5	285.7	515.2
4	220.5	272.1	492.6	401.6	326.4	728.0
5	202.3	333.7	536.0	275.1	364.2	639.3
6	184.3	252.1	436.4	315.5	321.7	637.2
7	223.5	220.9	444.4	341.0	368.1	709.1
8	175.5	321.0	496.5	306.5	409.7	716.2
9	269.7	313.7	583.4	351.3	389.2	740.5
10	283.1	311.2	594.3	360.4	487.3	847.7
11	249.7	338.8	588.5	327.6	371.4	699.0
12	225.5	282.0	507.5	416.8	334.4	751.2
13	229.5	262.1	491.6	282.9	308.9	591.8
14	237.9	246.2	484.1	294.3	304.4	598.7
15	268.3	266.4	534.7	311.5	348.7	660.2

Table A11: The measured delivery times for each individual patient. Delivery times for both arcs are included, as well as the total delivery time.

	6MV			FFF		
Patient (#)	arc1 [s]	arc2 [s]	Total [s]	arc3 [s]	arc4 [s]	Total [s]
1	74	80	154	73	82	155
2	79	83	162	79	88	167
3	71	77	148	72	77	149
4	76	83	159	76	82	158
5	74	80	154	74	82	156
6	71	77	148	72	77	149
7	75	84	159	77	81	158
8	76	88	164	78	86	164
9	79	82	161	76	78	152
10	76	85	161	76	82	156
11	81	86	167	74	84	158
12	73	81	154	72	78	150
13	76	80	156	75	85	160
14	81	83	164	73	78	151
15	78	78	156	73	77	150

Table A12: The RayStation estimated delivery times for each individual patient. Delivery times for both arcs are included, as well as the total delivery time.

	6MV			FFF		
Patient (#)	arc1 [s]	arc2 [s]	Total [s]	arc3 [s]	arc4 [s]	Total [s]
1	90	90	180	90	88	178
2	90	90	180	88	90	178
3	88	88	176	78	85	163
4	90	90	180	90	85	175
5	90	90	180	87	84	171
6	90	90	180	90	88	178
7	90	90	180	80	90	170
8	90	90	180	89	89	178
9	90	90	180	67	70	137
10	90	90	180	86	88	174
11	90	90	180	70	68	138
12	90	90	180	90	90	180
13	90	90	180	80	75	155
14	90	90	180	90	89	179
15	90	90	180	88	86	174

B

Matlab codes

```
% Bar graph OARs exceeding constraints (frequency)
c = categorical({'GTV-T+10mm (max 46.40 Gy)','Rectum (max 85% at 40 Gy)',
    'Rectum (max 95% at 30 Gy)','Bowel bag (max 250ccm at 40 Gy)',
    'Bowel bag (max 500ccm at 30 Gy)','Bowel bag (max 57.5 Gy)',
    'Femoral heads (max 50 Gy)','Bladder (max 75% at 40 Gy)',
    'Bladder (max 85% at 30 Gy)','Spinal canal (max 48 Gy)'});

figure()
barh(c,[15 15; 11 12; 11 12; 8 9; 6 9; 5 6; 4 4; 2 2; 2 2; 2 3])
title('OAR constraints exceeded');
xlabel('Frequency');
legend('6MV','FFF');
```

```
% Plotting abs. exceedings in Gy
x = [1.73,2.14,1.66,1.76,0.30,6.45,0.07,6.46,4.29,3.52,
    4.25,1.54,5.19,4.88,
    3.97,2.14,2.24,6.59,3.95,4.42,1.87,5.12,4.58,4.36,
    0.30,7.45,5.24,1.61,
    10.02,0.01,5.59,3.03,13.29,0.13,5.13,1.65,0.31,9.86,
    0.54,8.85,0.58,
    0.93,2.38,1.28,1.47,0.18,6.71,0.59,2.01,0.78,1.97,0.46,
    0.83,1.25,1.42,
    0.19,1.64,0.85,0.23,0.73,0.05,1.52,0.60,1.89,4.97,10.76,
    0.79,1.02,1.62,
    6.59,0.96,3.54,1.21,0.69,5.90,7.75,1.68,1.82,1.57,4.68,
    10.97,0.86,0.62,
```

```
    1.44,6.09,0.78,3.64,1.53,0.73,6.32,8.04,0.70,1.68,2.19,
    3.47,3.16,4.39,
    1.11,4.29,1.40,0.53,3.32,3.48,4.08,3.04,3.80,4.26,4.52,
    0.69,4.50,4.27,
    0.07,3.30,4.30,4.80,0.48,3.29,8.53,6.30,8.13,1.82,13.17,
    6.64,1.55,5.69,
    10.01,11.88,9.20,8.61,1.19,9.03,8.15,1.48,13.59,13.46,
    1.61,5.75,12.16,
    14.28,8.50,1.00,1.09,0.33,0.23,1.02];
group = [1,1,2,2,3,3,4,4,5,5,5,5,5,5,5,6,6,6,6,6,6,6,6,
    7,7,7,7,7,7,8,8,
    8,8,8,8,8,8,8,9,9,9,9,9,10,10,10,10,10,10,11,11,11,11,
    11,11,12,12,12,
    12,12,12,13,13,13,13,13,13,13,13,13,13,13,13,13,13,13,
    14,14,14,14,14,
    14,14,14,14,14,14,14,14,14,14,15,15,15,15,15,15,15,15,
    15,15,15,16,16,
    16,16,16,16,16,16,16,16,16,16,17,17,17,17,17,17,17,17,
    17,17,17,18,18,
    18,18,18,18,18,18,18,18,18,18,19,19,20,20,20];
positions = [1 1.25 2 2.25 3 3.25 4 4.25 5 5.25 6 6.25 7 7.25
    8 8.25 9 9.25
    10 10.25];

figure()
boxplot(x,group, 'positions', positions,'orientation', 'horizontal');
title('OAR constraints exceeded')
xlabel('Exceeded dose [Gy]')

set(gca,'ytick',[mean(positions(1:2)) mean(positions(3:4))
    mean(positions(5:6)) mean(positions(7:8)) mean(positions(9:10))
    mean(positions(11:12)) mean(positions(13:14)) mean(positions
        (15:16))
    mean(positions(17:18)) mean(positions(19:20))])
set(gca,'yticklabel',{'Bladder (max 75% at 40 Gy)',
    'Bladder (max 85% at 30 Gy)','Bowel bag (max 250ccm at 40 Gy)',
    'Bowel bag (max 500ccm at 30 Gy)','Bowel bag (max 57.5 Gy)',
```

```
    'Femoral heads (max 50 Gy)','GTV-T+10mm (max 46.4 Gy)',
    'Rectum (max 85% at 40 Gy)','Rectum (max 95% at 30 Gy)',
    'Spinal canal (max 48 Gy)'})

color = ['y', 'b', 'y', 'b','y', 'b', 'y', 'b','y', 'b', 'y', 'b', 'y'
    ,
    'b', 'y', 'b', 'y', 'b', 'y', 'b'];
h = findobj(gca,'Tag','Box');
for j=1:length(h)
   patch(get(h(j),'XData'),get(h(j),'YData'),color(j),'FaceAlpha',.5);
end

c = get(gca, 'Children');

hleg1 = legend(c(1:2), '6MV', 'FFF' );
xlim([0 15]);
```

```
% Plotting abs. exceedings in percent
x = [1.90,4.58,1.86,4.16,0.18,8.62,0.04,9.81,8.81,5.77,
    9.96,1.90,15,2.50,
    1.85,6.42,1.01,12.38,9.40,8.51,9.09,9.96,1.45,15,15,
    0.12,6.08,14.88,
    13.14,0.89,7.98,4.31,4.40,1.08,1.20,5,5,1.12,3.40,5,
    3.66,5,5,1.52,5,
    1.11,5,1.11,5,1.31,3.43,5,4.07,5];
group = [1,1,2,2,3,3,4,4,5,5,5,5,5,5,5,5,5,5,6,6,6,6,6,
    6,6,6,6,6,6,6,7,7,
    7,7,7,7,7,7,7,7,8,8,8,8,8,8,8,8,8,8,8,8];
positions = [1 1.25 2 2.25 3 3.25 4 4.25];

figure()
boxplot(x,group, 'positions', positions,'orientation', 'horizontal');
title('OAR constraints exceeded');
xlabel('[%]');
xlim([0 18]);
```

```
19
20 set(gca,'ytick',[mean(positions(1:2)) mean(positions(3:4))
21     mean(positions(5:6)) mean(positions(7:8))])
22 set(gca,'yticklabel',{'Bladder (max 75% at 40 Gy)',
23     'Bladder (max 85% at 30 Gy)','Rectum (max 85% at 40 Gy)',
24     'Rectum (max 95% at 30 Gy)'})
25
26 color = ['y', 'b', 'y', 'b','y', 'b', 'y', 'b'];
27 h = findobj(gca,'Tag','Box');
28 for j=1:length(h)
29    patch(get(h(j),'XData'),get(h(j),'YData'),color(j),'FaceAlpha',.5);
30 end
31
32 c = get(gca, 'Children');
33
34 hleg1 = legend(c(1:2), '6MV', 'FFF' );
```

```
1 % Plotting abs. exceedings in cm^3
2 x =
      [167.1,64.7,126.6,38.8,250.7,115.7,128.5,15.0,57.0,387.8,81.8,135.5,

3      49.7,245.9,107.7,205.0,5.6,325.3,204.0,46.4,313.9,0.2,206.5,115.9,
4      579.2,2.5,192.3,42.6,12.8,289.4,9.1,250.4];
5 group =
      [1,1,1,1,1,1,1,1,2,2,2,2,2,2,2,2,2,3,3,3,3,3,3,4,4,4,4,4,4,4,4,4];
6 positions = [1 1.25 2 2.25];
7
8 figure()
9 boxplot(x,group, 'positions', positions,'orientation', 'horizontal');
10 title('OAR constraints exceeded');
11 xlabel('[ccm^3]');
12
13 set(gca,'ytick',[mean(positions(1:2)) mean(positions(3:4))])
14 set(gca,'yticklabel',{'Bowel bag (max 250ccm at 40 Gy)',
15     'Bowel bag (max 500ccm at 30 Gy)'})
```

```
16
17 color = ['y', 'b', 'y', 'b'];
18 h = findobj(gca,'Tag','Box');
19 for j=1:length(h)
20    patch(get(h(j),'XData'),get(h(j),'YData'),color(j),'FaceAlpha',.5);
21 end
22
23 c = get(gca, 'Children');
24
25 hleg1 = legend(c(1:2), '6MV', 'FFF' );
```

```
1  % Pass rates 6MV
2  passrates_6MV_arc1 = [97.1 99.4 100 99.8 100 99.8 99.8 100 99.5 99.2
       100
3       95.9 99.8 97.8 99.0];
4  passrates_6MV_arc2 = [99.8 100 98.7 99.3 98.8 98.6 99.1 96.2 99.3 99.7
        99.8
5       96.0 99.8 97.6 100];
6  passrates_6MV_total = [98.3 99.9 99.9 99.4 100 100 98.6 99.0 99.7 99.8
        100
7       93.8 99.9 95.8 99.5];
8  % Pass rates FFF
9  passrates_FFF_arc3 = [98.5 96.0 98.9 96.8 98.7 96.8 94.9 98.9 98.8
       99.2
10      97.1 72.5 97.4 88.5 98.5];
11 passrates_FFF_arc4 = [98.0 94.2 100 98.8 97.7 96.5 95.3 99.6 99.4 96.6
        99.2
12      99.5 98.6 95.4 99.8];
13 passrates_FFF_total = [89.0 88.8 99.5 95.9 98.5 93.7 82.0 96.1 98.8
       95.1
14      98.6 94.5 98.4 89.6 96.2];
15
16 % Calculating mean and std 6MV
17 mean6_1 = mean(passrates_6MV_arc1);
18 mean6_2 = mean(passrates_6MV_arc2);
```

```
mean6_total = mean(passrates_6MV_total);
std6_1 = std(passrates_6MV_arc1);
std6_2 = std(passrates_6MV_arc2);
std6_total = std(passrates_6MV_total);
% Calculating mean and std FFF
meanF_1 = mean(passrates_FFF_arc3);
meanF_2 = mean(passrates_FFF_arc4);
meanF_total = mean(passrates_FFF_total);
stdF_1 = std(passrates_FFF_arc3);
stdF_2 = std(passrates_FFF_arc4);
stdF_total = std(passrates_FFF_total);

% Matrix with pass rates
passrates = [passrates_6MV_arc1; passrates_6MV_arc2;
    passrates_6MV_total;
     passrates_FFF_arc3; passrates_FFF_arc4; passrates_FFF_total];
passrates_trans = transpose(passrates); % transpose to get correct
    plot

% Assigning names to each sample
names = ["6MV arc1"; "6MV arc1"; "6MV arc1"; "6MV arc1"; "6MV arc1";
     "6MV arc1"; "6MV arc1"; "6MV arc1";
     "6MV arc1"; "6MV arc1"; "6MV arc1"; "6MV arc1"; "6MV arc1"; "6MV
        arc1";
     "6MV arc1";
     "6MV arc2"; "6MV arc2"; "6MV arc2"; "6MV arc2"; "6MV arc2"; "6MV
        arc2";
     "6MV arc2";
     "6MV arc2"; "6MV arc2"; "6MV arc2"; "6MV arc2"; "6MV arc2"; "6MV
        arc2";
     "6MV arc2"; "6MV arc2";
     "6MV total"; "6MV total"; "6MV total"; "6MV total"; "6MV total";
     "6MV total"; "6MV total"; "6MV total";
     "6MV total"; "6MV total"; "6MV total"; "6MV total"; "6MV total";
     "6MV total"; "6MV total";
     "FFF arc3"; "FFF arc3"; "FFF arc3"; "FFF arc3"; "FFF arc3"; "FFF
        arc3";
```

```
50      "FFF arc3";
51      "FFF arc3"; "FFF arc3"; "FFF arc3"; "FFF arc3"; "FFF arc3"; "FFF
            arc3";
52      "FFF arc3"; "FFF arc3";
53      "FFF arc4"; "FFF arc4"; "FFF arc4"; "FFF arc4"; "FFF arc4"; "FFF
            arc4";
54      "FFF arc4";
55      "FFF arc4"; "FFF arc4"; "FFF arc4"; "FFF arc4"; "FFF arc4"; "FFF
            arc4";
56      "FFF arc4"; "FFF arc4";
57      "FFF total"; "FFF total"; "FFF total"; "FFF total"; "FFF total";
58      "FFF total"; "FFF total"; "FFF total";
59      "FFF total"; "FFF total"; "FFF total"; "FFF total"; "FFF total";
60      "FFF total"; "FFF total"];
61
62  namesGrp = char(names);
63
64  % Boxplot
65  figure()
66  boxplot(passrates_trans, namesGrp);
67  title('Gamma pass rates');
68  xlabel('');
69  ylabel('Pass rate [%]');
```

```
1  c = categorical({'01','02','03','04','05','06','07','08', '09','10','
       11',
2       '12','13','14','15'});
3
4  figure()
5  barh(c,[98.3 89.0; 99.9 88.8; 99.9 99.5; 99.4 95.9; 100 98.5; 100
       93.7;
6       98.6 82.0; 99.0 96.1; 99.7 98.8; 99.8 95.1; 100 98.6; 93.8 94.5;
            99.9
7       98.4; 95.8 89.6; 99.5 96.2]);
8  title('Individual gamma pass rates');
```

```
xlabel('Pass rate [%]');
ylabel('Patient number');
legend('6MV','FFF');
xlim([80 105]);
```

```
% MU (6MV and FFF arcs)
mu6MVarcs = [202.32 269.70 223.54 184.34 283.14 229.49 220.53 175.45 249.72
    274.73 237.93 268.25 232.28 225.53 178.04 333.70 313.65 220.94 252.05
    311.17 262.05 272.14 321.01 338.81 254.70 246.21 266.39 282.25 281.97
    224.83];
muFFFarcs = [275.11 351.26 341.03 315.46 360.39 282.85 401.55 306.50 327.63
    364.82 294.26 311.54 272.43 416.84 229.49 364.20 389.20 368.06 321.69
    487.33 308.91 326.38 409.66 371.41 452.03 304.44 348.71 539.22 334.36
    285.72];

% Total MUs
mu6MV = mu6MV_arc1 + mu6MV_arc2;
muFFF = muFFF_arc3 + muFFF_arc4;

% Assigning names
names = ["6MV"; "6MV"; "6MV"; "6MV"; "6MV"; "6MV"; "6MV"; "6MV"; "6MV";
    "6MV"; "6MV"; "6MV"; "6MV"; "6MV"; "6MV"; "FFF"; "FFF"; "FFF"; "FFF";
    "FFF"; "FFF"; "FFF"; "FFF";"FFF"; "FFF"; "FFF"; "FFF"; "FFF";
    "FFF"];

% Matrix containing the MUs
```

```
mu_pre = [mu6MV; muFFF];
mu = transpose(mu_pre); % transpose for correct plotting
namesGrp= char(names);

% Boxplot
figure()
boxplot(mu, namesGrp);
title('Monitor units for 6MV and FFF beams');
xlabel('');
ylabel('MUs');

% Scatter plot (6MV vs FFFs)
figure()
scatter(mu6MV, muFFF ,'bl', '*');
title('Monitor units (6MV vs FFF)');
xlabel('6MV');
ylabel('FFF');
axis([375 900 375 900]);
refline(1,0); % Constructing reference unity line

[p1,h1] = signrank(mu6MV, muFFF) % Wilcoxon test for total MUs
[p2,h2] = signrank(mu6MVarcs, muFFFarcs) % Wilcoxon test for arcs MU
```

```
% MUs of each arc
muFFF_arc3 = [275.11 351.26 341.03 315.46 360.39 282.85 401.55 306.50
    327.63 364.82 294.26 311.54 272.43 416.84 229.49];
muFFF_arc4 = [364.20 389.20 368.06 321.69 487.33 308.91 326.38 409.66
    371.41 452.03 304.44 348.71 539.22 334.36 285.72];
muFFF = muFFF_arc3 + muFFF_arc4; % total MUs FFF
mu6MV_arc1 = [202.32 269.70 223.54 184.34 283.14 229.49 220.53 175.45
    249.72 274.73 237.93 268.25 232.28 225.53 178.04];
mu6MV_arc2 = [333.70 313.65 220.94 252.05 311.17 262.05 272.14 321.01
    338.81 254.70 246.21 266.39 282.25 281.97 224.83];
mu6MV = mu6MV_arc1 + mu6MV_arc2; % total MUs 6MV

```

```
% Pass rates
pass_6MV_arc1 = [100 99.5 99.8 99.8 99.2 99.8 99.8 100 100 97.1 97.8
    99.0
 99.4 95.9 100];
pass_6MV_arc2 = [98.8 99.3 99.1 98.6 99.7 99.8 99.3 96.2 99.8 99.8
    97.6
 100 100 96.0 98.7];
pass6MV = [100 99.7 98.6 100.0 99.8 99.9 99.4 99.0 100 98.3 95.8 99.5
 99.2 93.8 99.9];
pass_FFF_arc3 = [98.7 98.8 94.9 96.8 99.2 97.4 96.8 98.9 97.1 98.5
    88.5
 98.5 96.0 72.5 98.9];
pass_FFF_arc4 = [97.7 99.4 95.3 96.5 96.6 98.6 98.8 99.6 99.2 98.0
    95.4
 99.8 94.2 99.5 100];
passFFF = [98.5 98.8 82.0 93.7 95.1 98.4 95.9 96.1 98.6 89.0 89.6 96.2
 88.8 94.5 99.5];

% Plotting MU vs pass rate (6MV)
figure()
scatter(mu6MV_arc1, pass_6MV_arc1,'bl', '*');
title('Monitor units vs pass rate (6MV beams)');
xlabel('MUs');
ylabel('Pass rate [%]');
hold on
scatter(mu6MV_arc2, pass_6MV_arc2,'r', '*');
legend('arc1','arc2');
axis([160 350 70 105]);

% Plotting MU vs pass rate (FFF)
figure()
scatter(muFFF_arc3, pass_FFF_arc3,'bl', '*');
title('Monitor units vs pass rate (FFF beams)');
xlabel('MUs');
ylabel('Pass rate [%]');
hold on
scatter(muFFF_arc4, pass_FFF_arc4,'r', '*');
```

```
legend('arc3','arc4');
axis([200 550 70 105]);

% Making trend lines
p1 = polyfit(mu6MV,pass6MV,1);
f1 = polyval(p1,mu6MV);

p2 = polyfit(muFFF,passFFF,1);
f2 = polyval(p2,muFFF);

% Plotting with trend lines
figure()
scatter(mu6MV, pass6MV,'bl', '*');
title('Total monitor units vs total pass rate');
xlabel('MUs');
ylabel('Pass rate [%]');
hold on
scatter(muFFF, passFFF,'r', '*');
hold on
plot(mu6MV,f1,'-');
hold on
plot(muFFF,f2,'-');
axis([350 900 80 103]);
legend('6MV','FFF','Trend line 6MV','Trend line FFF');
```

```
% Measured delivery times
time6MV_arc1 = [74 79 71 76 74 71 75 76 79 76 81 73 76 81 78];
time6MV_arc2 = [80 83 77 83 80 77 84 88 82 85 86 81 80 83 78];
timeFFF_arc3 = [73 79 72 76 74 72 77 78 76 76 74 72 75 73 73];
timeFFF_arc4 = [82 88 77 82 82 77 81 86 78 82 84 78 85 78 77];

% RayStation estimated delivery times
RS6MV_arc1 = [90 90 88 90 90 90 90 90 90 90 90 90 90 90 90];
RS6MV_arc2 = [90 90 88 90 90 90 90 90 90 90 90 90 90 90 90];
RSFFF_arc3 = [90 88 78 90 87 90 80 89 67 86 70 90 80 90 88];
```

```
RSFFF_arc4 = [88 90 85 85 84 88 90 89 70 88 68 90 75 89 86];

% Scatter plot delivery times (6MV vs FFF)
figure
scatter(time6MV_arc1, timeFFF_arc3,'bl', '*');
title('Delivery times (6MV vs FFF)');
xlabel('6MV [s]');
ylabel('FFF [s]');
hold on
scatter(time6MV_arc2, timeFFF_arc4,'r', '*');
refline(1,0);
legend('arc1 vs arc3', 'arc2 vs arc4','(x = y)');
axis([70 91 70 91]);


% Figure 6MV
figure
scatter(RS6MV_arc1, time6MV_arc1,'bl', '*');
title('Delivery time 6MV (RayStation vs measured)');
xlabel('RayStation delivery time [s]');
ylabel('Measured delivery time [s]');
hold on
scatter(RS6MV_arc2, time6MV_arc2,'r', '*');
legend('arc1','arc2','x = y');
axis([70 95 70 95]);

% Figure FFF
figure
scatter(RSFFF_arc3, timeFFF_arc3,'bl', '*');
title('Delivery time FFF (RayStation vs measured)');
xlabel('RayStation delivery time [s]');
ylabel('Measured delivery time [s]');
hold on
scatter(RSFFF_arc4, timeFFF_arc4,'r', '*');
refline(1,0);
legend('arc3','arc4','x = y');
axis([65 95 65 95]);
```

```
48
49 % Total delivery time
50 time6MV = time6MV_arc1 + time6MV_arc2;
51 timeFFF = timeFFF_arc3 + timeFFF_arc4;
52
53 figure
54 scatter(time6MV, timeFFF,'bl', '*');
55 title('Total delivery times (6MV vs FFF)');
56 xlabel('6MV [s]');
57 ylabel('FFF [s]');
58 hold on
59 refline(1,0);
60 legend('Measured data', '(x = y)');
61
62 % Wilcoxon signed rank test
63 realTime6MVarcs = [74 79 71 76 74 71 75 76 79 76 81 73 76 81 78 80 83
       77 83
64     80 77 84 88 82 85 86 81 80 83 78];
65 realTimeFFFarcs = [73 79 72 76 74 72 77 78 76 76 74 72 75 73 73 82 88
       77 82
66     82 77 81 86 78 82 84 78 85 78 77];
67
68 [p1,h1] = signrank(realTime6MVarcs, realTimeFFFarcs) % Wilcoxon 6MV vs
       FFF
69 [p2,h2] = signrank(time6MV,timeFFF) % Wilcoxon total delivery times
```

```
1 % PTV volumes
2 volume_PTV = [2011.54 1787.56 1957.08 2209.12 2212.24 1426.20 2546.02
3     1967.47 2002.40 1741.75 2193.84 1828.56 1040.70 2023.31 1610.81];
4 volume_boost = [119.37 116.94 41.10 193.67 90.82 31.24 140.69 107.32
      89.76
5     83.20 153.45 80.66 57.13 80.42 90.37];
6 volume = volume_PTV + volume_boost; % Total PTV volume
7
8 % Pass rates
```

```
pass_6MV = [98.3 99.9 99.9 99.4 100 100 98.6 99.0 99.7 99.8 100 93.8 99.9
    95.8 99.5];
pass_FFF = [89.0 88.8 99.5 95.9 98.5 93.7 82.0 96.1 98.8 95.1 98.6 94.5
    98.4 89.6 96.2];

% Making trend lines
p1 = polyfit(volume,pass_6MV,1);
f1 = polyval(p1,volume);
p2 = polyfit(volume,pass_FFF,1);
f2 = polyval(p2,volume);

% Plotting
figure
scatter(volume, pass_6MV,'bl', '*');
title('Total PTV volume vs total gamma pass rate');
xlabel('Total PTV volume [cm^3]');
ylabel('Pass rate [%]');
axis([1000 2600 80 101]);
hold on
scatter(volume, pass_FFF,'r', '*');
hold on
plot(volume,f1,'-');
plot(volume,f2,'-');
legend('6MV','FFF','Trend line 6MV','Trend line FFF');

% Relative PTV boost volumes
volume_boost_rel = volume_boost./volume;

% Making trend lines
p3 = polyfit(volume_boost_rel,pass_6MV,1);
f3 = polyval(p3,volume_boost_rel);
p4 = polyfit(volume_boost_rel,pass_FFF,1);
f4 = polyval(p4,volume_boost_rel);

% Plotting rel. boost volume
```

```
figure
scatter(volume_boost_rel, pass_6MV,'bl', '*');
title('Relative PTV boost volume vs total gamma pass rate');
xlabel('Relative PTV boost volume');
ylabel('Pass rate [%]');
axis([0 0.1 80 105])
hold on
scatter(volume_boost_rel, pass_FFF,'r', '*');
hold on
plot(volume_boost_rel,f3,'-');
plot(volume_boost_rel,f4,'-');
legend('6MV','FFF','Trend line 6MV','Trend line FFF');
```